Specialisation of ribosomes in gonads through paralog-switching

Tayah Hopes[1,2], Michaela Agapiou[1,2], Karl Norris[1,2,3], Charley G.P. McCarthy[4], Mary J O'Connell[4], Juan Fontana[1,3 *], Julie L Aspden[1,2 *]

1 School of Molecular and Cellular Biology, Faculty of Biological Sciences, University of Leeds, LS2 9JT, UK.

2 LeedsOmics, University of Leeds, UK

3 Astbury Centre for Structural Molecular Biology, University of Leeds, Leeds, LS2 9JT, UK.

4 School of Life Sciences, Faculty of Medicine and Health Sciences, The University of Nottingham, Nottingham, NG7 2UH, UK.

* For correspondence: j.aspden@leeds.ac.uk; j.fontana@leeds.ac.uk

Abstract

Ribosomes have long been thought of as homogeneous, macromolecular machines but recent evidence suggests they are heterogeneous and their specialisation can regulate translation. Here, we have characterised ribosomal protein heterogeneity across 5 tissues of *Drosophila melanogaster*. We find that testis and ovary contain the most heterogeneous ribosome populations, and that specialisation in these tissues occurs through paralog-switching. For the first time, we have solved structures of ribosomes purified from *in vivo* tissues by cryo-EM, revealing differences in precise ribosomal arrangement for testis and ovary 80S ribosomes. Differences in the amino acid composition of paralog pairs and their localisation on the ribosome exterior indicate paralog-switching could alter the ribosome surface, enabling different proteins to regulate translation. One testis-specific paralog-switching pair is also found in humans, suggesting this is a conserved site of ribosome specialisation. Overall, this work allows us to propose possible mechanisms by which ribosome specialisation can regulate translation.

Introduction

Protein synthesis is essential across the tree of life and undertaken by the highly conserved macromolecular complex of "the ribosome". mRNA translation is regulated at many levels, but until recently the ribosome itself was not thought to be part of this control system. Recent studies have suggested that ribosomes can contribute to gene expression regulation, through specific changes in their composition, i.e. specialisation [1-3]. These specialised ribosomes are thought to contribute to the translation of specific mRNA pools; but the mechanism by which this takes place is yet to be understood.

Previous analysis in a variety of organisms (mouse [1], yeast [4], and humans [5]) has shown that the composition of ribosomes is not homogeneous. In fact, specialisation of ribosomes is thought to be able to occur through a) additional protein components [6], b) substitution of ribosomal protein (RP) paralogs [7], c) post-translational modification of RPs [8], and d) rRNA modifications [9]. All these changes to the composition of ribosomes potentially contribute to ribosome specialisation.

Two significant factors have contributed to the logic behind the idea of 'specialised ribosomes'; a) prevalence of tissue specific RP expression and b) distinctive phenotypes when RP genes are disrupted [10]. Many RPs exhibit differences in expression levels across various tissues in mammals [1, 5, 11], plants [12], and insects [7]. For example, RpS5A and RpS5B are expressed in different cell types during early *Arabidopsis thaliana* development [13]. Disrupted RP genes result in varied, distinctive phenotypes suggesting that not all components are equally important all the time. For example, RpL38 mouse mutants exhibit a homeotic transformation phenotype with few other effects [1], whilst RpL38 mutants in *D. melanogaster* exhibit large wings, small bristles, delayed development and disorganised wing hair polarity [14].

Human cytoplasmic ribosomes usually comprise of 80 RPs and 4 rRNAs. This is similar across the majority of multicellular eukaryotes including *D. melanogaster* with 80 RPs and 5 rRNAs. However, annotated in FlyBase there are 93 cytoplasmic RP genes, including 39 small subunit proteins and 54 large subunit proteins [15]. These additional genes code for 13 paralogs in *D. melanogaster*. In fact, across eukaryotes many RP genes possess paralogs, for example human RpL3 and RpL3L [11] and *Arabidopsis* RpS8A and RpS8B [13]. In total, there are 19 pairs of paralogs in humans [4] and all 80 RPs in *Arabidopsis thaliana* have paralogs [16].

To dissect the function of ribosome heterogeneity it is necessary to understand biological importance within context of whole organisms. Within the developmental biology field, a large proportion of research focuses on the contribution of transcription to gene expression control. However, during development a variety of processes and key time points are highly dependent on the regulation of mRNA translation (oogenesis in *Xenopus* [17], early embryo development in *Drosophila* [18] and mammalian erythropoiesis [19]). The balance between self-renewal and differentiation at the stem cell niche is highly dependent on translation in both the ovary and the testis [20]. This is exemplified by disruptions to the stem cell niche in the testis when RPs are knocked down e.g. RpL19 RNAi results in over-proliferation of early germ cells in *D. melanogaster* [21]. During the meiotic phase of gametogenesis, transcription does not occur [22]; therefore meiotic cells rely on post-transcriptional gene regulation [23]. The translational machinery has evolved to become specialised within the testis with various testis specific components e.g. eIF4E-3 in *D. melanogaster* [24]. Many of the RP mutants associated with the *Minute* phenotypes have impaired fertility in both males and females [25, 26]. Moreover, mutations in 64 RPs in *D. melanogaster* result in *Minute* phenotypes of some sort [27].

Several human diseases have been attributed to mutations in RP genes. These diseases are called ribosomopathies, and they result from impaired translation and/or extra-ribosomal RP functions. The clinical symptoms vary between different RPs, suggesting human RPs also possess specialised functions, likely with respect to their contribution to the translation of specific mRNA pools. For example, mutations in RpS19 result in Diamond-Blackfan anaemia (DBA): a condition that presents with pure red cell aplasia [28].

Here we hypothesise that specialised ribosomes exist in the *D. melanogaster* testis to provide an additional level of mRNA translational regulation during spermatogenesis. Thus, we set out to determine potential changes to the ribosome and its function by probing the protein composition in 3 tissues (head, testis and ovary), during development in the embryo and embryo derived tissue culture S2 cells in *D. melanogaster*. Using quantitative mass spectrometry we identified heterogeneous ribosome populations, especially in the gonads. The main source of this variation in ribosome composition is paralog-switching, occurring in up to 50% of ribosomes in the testis and the ovary for specific paralogs. We found little difference in composition between single 80S ribosomes and, the more translationally active, polysome ribosomes from the same tissue, apart from in the ovary, where 2 paralogs are more abundant in 80S ribosomes. We solved structures of different ribosome populations to understand the potential mechanistic impact of these paralog-switching events. The resultant structures suggest potential mechanisms of translational regulation by different paralogs within the ribosome. To understand the broader importance of specialisation through paralog switching events we analysed the levels of conservation between paralog pairs. RpL22 has a duplicate RpL22L in mammals (including humans), and RpL22-like in *Drosophila,* these duplication events have occurred independently suggesting that it may represent a common mechanism of specialisation across a range of organisms and ribosomes.

Results

Heterogeneous ribosome populations exist in different tissues

Many eukaryotic genomes contain numerous RP paralogs and their contribution to ribosomal function is poorly understood. In *D. melanogaster* there are 93 RP genes (FlyBase), which includes 13 pairs of paralogs, normally resulting in 80 proteins in each ribosome [29]. The expression of RPs and

specifically RP paralogs has been reported to vary in a tissue specific manner. To profile potential differences in expression in *D. melanogaster* we analysed publicly available RNA-Seq data across various developmental time points and tissues. Hierarchical clustering of RP mRNA abundances across these different biological samples reveals variations in expression of RP mRNAs between tissues, with a cluster of RPs with much higher expression in the testis compared to other tissues (Fig 1A). This includes RpL22-like, a paralog of RpL22 previously reported as a testis specific ribosomal protein [7]. These results suggest the presence of testis-specific translational machinery.

To determine whether these different RPs are translated and incorporated into ribosomes we assessed the protein composition of ribosomes from these same tissues and cells; testes, ovaries, heads (mixture of male and female), embryos (0-2hr) and S2 cells (derived from embryo). Ribosomal complexes were purified using sucrose gradients and ultracentrifugation (Fig 1B). Both 80S and polysome complexes were isolated. The relative amounts of ribosomes existing as 80S or polysome complexes varied substantially across the samples (Sup 1A-E). Both monosome (80S) and polysome fractions were isolated for each tissue/cell type in two independent experiments before being subjected to quantitative mass spectrometry (Tandem Mass Tag; TMT). Overall correlation between the two biological replicates is high as the global protein content in testis 80S samples had a Pearson's correlation coefficient of 0.93 (Fig 1C). Similar results are obtained when considering only ribosomal proteins (Sup 1F & G) and across samples (Sup 1H-K).

To understand differences in ribosome composition between the tissues, protein abundances of ribosomal proteins were subject to hierarchical clustering (Fig 1D). A cluster of proteins emerged, which were enriched in the testis 80S ribosomes compared to 80S ribosomes from other tissues. This cluster included RpL22-like, RpL37b, RpS19b, RpS10a and RpS28a, RpS15Ab. There was also an ovary 80S enriched cluster of ribosomal proteins, RpL24-like, RpL7-like and RpL0-like (Fig 1D). PCA of protein abundances by ribosomal protein revealed that the majority of RPs (75/93) form a group together, suggesting they are incorporated in all ribosomes. The expression of RpL22-like, RpL37b, RpS19b, RpS10a and RpS28a clusters together, as their incorporation pattern across the different tissues is similar and this is driven mainly by their differential presence in testis 80S (Fig 1E, inset). The same can also be seen in the ovary enriched proteins (Fig 1E, inset).

When ribosomal protein abundances are plotted between different 80S complexes, we report that the largest differences are from paralogs rather than canonical RPs (Fig 1F & G). Comparison of testis 80S and head 80S shows 6 paralogs (RpL22-like, RpL37b, RpS19b, RpS10a, RpS28a and RpS15Ab) are highly enriched in the testis 80S compared to head (Fig 1F), whilst RpS11 is enriched in the head 80S. Comparison of testis 80S and ovary 80S reveals that whilst the majority of ribosomal proteins correlate between the two gonads, the same paralogs enriched in testis 80S compared to head were also enriched compared to ovary (Fig 1G). RpL24-like, RpL7-like, RpL0-like and RpS5b are all far more abundant in ovary 80S ribosomes than in the testis (Fig 1G). Overall, specialisation seems most common in the gonads and we identify both testis- and ovary-enriched paralogs.

Ribosomal protein paralogs contribute to ribosome heterogeneity

There are 13 pairs of RP paralogs in the *D. melanogaster* genome and from our TMT data we can see the majority are both expressed and incorporated into 80S ribosome in at least one of the analysed tissues or the developmental time point of the embryo. Hierarchical clustering of these paralogs re-emphasises the existence of gonad specific ribosomal complexes (Fig 2A). To understand the relationship between each of the two paralogs we used the mass spectrometry data to quantify relative abundances of the two paralogs with the matched pairs within the various tissues. Interestingly, for the majority of these proteins one of the paralogs seems to be dominant in terms of its presence in 80S ribosomes (Fig 2B). Strikingly the testis differs in composition the most when compared to the other samples (Fig 2A & B). In total, we find ~60% of testis 80S ribosomes contain RpL22-like rather than RpL22. These patterns were seen with both TMT experiments (Sup 2A). For 5 paralog pairs the second paralog is most abundant in the testis, and low in other samples (RpL22-like, RpL37b, RpS19b, RpS10a, RpS28a), we term these 'testis-enriched paralogs'. A similar situation

153 is seen for 4 paralog pairs where the second paralog is most abundant in the ovary (RpL24-like,
154 RpL7-like, RpL0-like and RpS5b), 'ovary-enriched paralogs'. Interestingly RpS5b is present in ~50% of
155 ovary 80S ribosomes, 45% of embryo 80S ribosomes and 30% of testis 80S ribosomes. Thus, RpS5b
156 has an unusually broad incorporation across the different sampled ribosomes.
157
158 **Differences in ribosome composition are mainly the result of selective protein incorporation**
159 To understand the expression of RP paralogs, we analysed mRNA-Seq levels of each of the
160 paralog pairs (Sup 2B). When relative paralog pair expression is profiled as a percentage on the basis
161 of RNA-Seq, it is clear that differences in protein composition of ribosomes is not purely driven by
162 transcriptional control of paralog genes (Sup 2B). We directly compared RP RNA expression (RNA-
163 Seq) and RP protein incorporation (ribosome-TMT) identifying when RP incorporation into the
164 ribosome does not correlate with mRNA expression level (Fig 2C). Specifically, RpL24-like is
165 transcribed across all tissues at substantial levels (Sup 2B) and there is no difference in mRNA level
166 between ovary and testis. However, RpL24-like is far more abundant in ovary 80S than testis 80S (Fig
167 2C) and is only represented in ovary 80S ribosomes (Fig 2B). RpL34a is very lowly incorporated into
168 all ribosomes (Fig 2B) but its mRNA is expressed across tissues at substantial levels (Sup 2B). The
169 opposite is true for RpS15Ab, whose RNA levels are similarly low between testis and ovary but is
170 preferentially incorporated into testis 80S (Fig 2C). RpL7-like is expressed at the RNA level broadly in
171 substantial amounts (Sup 2B) but is only incorporated into ribosomes at very low levels compared to
172 RpL7 (<10%). Of note, the differential incorporation of RpL22-like into testes ribosomes compared to
173 ovaries is driven by a transcriptional difference between the two tissues (Fig 2C, Sup 2B).
174
175 **Composition of 80S ribosomes and polysomal ribosomes is similar**
176 There is conflicting evidence as to the functionality or translational activity of monosomes
177 (80S ribosomes), some suggest that these ribosomes are actively translating [30] whilst others
178 suggest that not all 80S ribosomes are engaged in active translation [31]. To determine if there was
179 any difference in ribosome composition between monosomes and polysome complexes, we
180 compared the two by TMT. In general, there is very little difference in RP composition between 80S
181 ribosomes and polysomes, e.g. testis (Fig 3A), head (Sup 3A). However, there are two paralogs
182 enriched in the ovary 80S compared to the ovary polysome, RpL7-like and RpL24-like (Fig 3B). Such a
183 large enrichment of these two paralogs in 80S complexes suggests that they potentially represent
184 ribosome complexes whose activity is being regulated. Therefore, these 80S complexes may not be
185 as translationally active as the polysome complexes. When the composition of ovary and testis
186 polysomes are compared we identify 6 testis-enriched RPs, which are all paralogs; RpL22-like,
187 RpL37b, RpS19b, RpS10a, RpS28a and RpL15Ab (Fig 3C). In fact, these are the same proteins
188 enriched in testis 80S compared to ovary 80S (Fig 1G). In this comparison we also identify a group of
189 proteins slightly enriched in the ovary polysomes; RpL37a, RpL22, RpS5b, RpL0-like and RpL40 (Fig
190 3C). Compared to the testis paralogs this fits well with the paralog switching between RpL37a/b,
191 RpS5a/b and RpL22/RpL22-like. When the relative composition of polysomes for paralog pairs was
192 determined the overall pattern was similar to 80S (Sup 3B). Differential incorporation within paralog
193 pairs (Fig 3D) highlights the main differences between 80S and polysomes are associated with
194 ovaries, and are RpL24/24-like, RpL7/7-like.
195
196 **Cryo-electron microscopy of testis and ovary ribosomes reveals a mechanism for inactivation of**
197 **testis 80S ribosomes**
198 To understand the molecular implications of the paralog switching events we identified by
199 mass spectrometry, we sought to solve structures of different ribosome populations. Ribosomal
200 complexes were isolated in the same way as was previously described for TMT by sucrose gradient
201 centrifugation (Fig 1B), with an additional step to concentrate purified samples (see Methods).
202 Imaging the sample by cryo-electron microscopy (cryo-EM) confirmed that the ribosome complexes
203 were highly pure and concentrated (Sup 4A). Testis 80S ribosomes were applied to grids and a

204 dataset containing ~47,000 particles was collected. Three-dimensional classification of this testis 80S
205 dataset identified a single structurally distinct class of 80S ribosomes, which was refined to an
206 average at 3.5 Å resolution (Fig 4A and Sup 4B). This provided a substantial improvement to the only
207 other *D. melanogaster* ribosome cryo-EM average at 6 Å resolution, from embryos [29]. We
208 performed a similar experiment with ovary 80S ribosome preparations, collecting a dataset
209 containing ~200,000 particles, and resulting in an average at 3.0 Å resolution (Fig 4B; Sup 4C & D).
210 These averages allowed us to generate atomic models for testis and ovary 80S ribosomal complexes
211 (Sup Table 1).
212 Comparison of the testis and ovary averages revealed that the main difference between
213 them was at the P/E tRNA site (Fig 4A and B). While the ovary 80S average did not contain any
214 densities in this region, the testis 80S average contained densities that did not correspond to a tRNA
215 (Fig 4A, circle). As a comparison, the previously published *D. melanogaster* average contained
216 densities for an E-tRNA and for elongation factor 2, both of which are not present in our averages.
217 By combining information from the testis 80S structure and the corresponding TMT data, we
218 identified this density to be CG31694-PA (Fig 4C), which is highly abundant in the testis 80S
219 complexes (10,451 normalised abundance, see Methods; 54th most abundant protein in testis 80S).
220 CG31694-PA is an ortholog of IFRD2, identified in translationally inactive rabbit ribosomes as being
221 bound to P/E sites of ~20% 80S isolated from rabbit reticulocytes [32]. Strikingly, in the reticulocytes
222 the presence of IFRD2 is always accompanied by a tRNA in a noncanonical position (termed Z site), in
223 the testis 80S average no tRNA was found in this region. In mammals IFRD2 is thought to have a role
224 in translational regulation during differentiation. Differentiation is a key process during
225 spermatogenesis within the testis, and in this context it is unsurprising to have found this protein in
226 the testis 80S. CG31694-PA has considerable amino acid sequence conservation with IFRD2, 32%
227 identity (Sup 4E & F). The presence of CG31694-PA suggests that a significant proportion of the testis
228 80S ribosomes is in fact not actively engaged in translation. CG31694-PA density was not present in
229 the ovary 80S structure suggesting far fewer ribosomes are inactive by this mechanism in the ovary
230 (5,105 normalised abundance in ovary 80S TMT compared with 10,451 in testis 80S). The presence
231 of CG31694-PA does not affect the paralog switching events because these events were identical
232 between the testis 80S and testis polysome ribosomes. To verify this, we solved the structure of
233 ribosomes isolated from testis polysomes (cryo-EM average resolution was 4.9 Å) (Fig 4D and Sup
234 4G-I). It is clear from the density map that CG31694-PA is not present in the P/E sites; rather there is
235 density for the E-tRNA in these actively translating ribosomes (Fig 4C & D). The TMT data indicates
236 that levels of CG31694-PA are higher in the testis 80S than the testis polysomal complexes (10,451
237 normalised abundance in 80S compared to 6,144 in polysomes, see methods).
238
239 **Functional implications of paralog switching event in gonads**
240 By mapping the paralog switching events onto our ribosome structures we identified three
241 clusters of paralogs undergoing switching. 1) Paralogs within the small subunit, including RpS19a/b
242 and RpS5a/b, map to the head of the 40S near the mRNA channel (Fig 5A & B). 2) Paralogs within the
243 large subunit tend be surface-exposed. Specifically, RpL22/RpL22-like and RpL24/RpL24-like locate
244 towards the back of the ribosome (Fig 5C & D). 3) Paralogs that are located in ribosome stalks, RpLP0
245 and RpL10A, potentially interacting with the mRNA during translation (Fig 5E). Of note, the small
246 subunit paralogs are close to the mRNA channel, pointing towards functional differences in mRNA
247 selectivity of the ribosome.
248 By comparing the atomic models for testis 80S and ovary 80S, we identified differences
249 between switched paralogs (Table 1). Specifically, the three paralogs with the greatest proportion
250 (RpL22-like, 60% abundant in testis 80S; RpS19b, close to 50% abundant in testis 80S; and RpS5b,
251 over 50% abundant in ovary 80S; Fig 2B) showed the largest differences in their atomic models
252 (Fig 6A-F). Additionally, of the paralogs that do not switch between testis 80S and ovary 80S, RpS28b
253 showed the largest differences (Fig 6G & H). This is probably due to its proximity to CG31694-PA
254 (Fig 6I).

Comparing the amino acid sequences of each paralog pair it is possible to predict that they might contribute different functionality to the ribosome (Table 2, Sup 6A-J and Sup 7A-H). RpL22 and RpL22-like are only 45% identical, even though they are very similar in length (Fig 7A, Sup 7A). Unfortunately, the most different region between RpL22 and RpL22-like (i.e., the N-terminal region; Fig 7A), faces the exterior of the ribosome and is not resolved in the cryo-EM density (Fig 7A shows in bold the regions of RpL22 and RpL22-like present in the ovary 80S and testis 80S reconstructions, respectively). It is possible to imagine that given the majority of these paralogs are localised to the exterior of the ribosome, by switching one for the other might provide a difference exterior surface with which other associated factors might bind and change.

Conservation of paralog switching and implications for human disease

To probe how widespread paralog switching events might be to facilitate ribosome specialisation we determined the level of conservation of RpL22 and RpL22-like in other animal genomes. Orthologs of RpL22 were identified across a range of animals including Drosophilid*s*. We determined that the paralogous pair RpL22 and RpL22-like present in *D. melanogaster* evolved by 3 independent duplication events across the animal clade (Fig 7B). A duplication event unique to the drosophila clade produced the paralogous pair RpL22 and RpL22-like that are identifiable in 6 out of the 12 Drosophila species sampled. The additional 2 duplication events present in the vertebrate clade may be the result of whole genome duplication rather than individual gene duplication events. The first of these vertebrate duplications produced the paralog pair RpL22 and RpL22L we observe in humans for example. The second vertebrate RPL22 duplication specific event occurred amongst teleost fishes and the most parsimonious explanation of pattern of distribution of duplicate copies would suggest subsequent lost in some lineages (Fig 7B). Thus, RPL22 has undergone multiple independent duplication events, generating a complex array of paralogous pairs.

Discussion

We have characterised the heterogeneity of ribosome composition across *Drosophila melanogaster* tissues and the developmental time point of embryos. For the first time we have identified differences in 80S ribosome composition purified from *in vivo* tissues. The main source of heterogeneity we discovered were paralog-switching events in the gonads. We have identified five testis-specific paralogs (RpL22-like, RpL37b, RpS19b, RpS10a, Rp28a) and four ovary-enriched paralogs (RpL24-like, RpL7-like, RpL0-like and RpS5b), which includes paralog, RpS5b, which is also to a lesser extent present in embryo and testis. There are very few differences between the composition of 80S and polysome ribosomes across all tissues. The exception to this is an enrichment of RpL24-like and RpL7-like in ovary 80S ribosomes compared to polysome ribosomes. These results are, in general, not just the consequence of transcriptional regulation of these paralogous genes. Rather there is modulation at the level of the translation of these proteins or incorporation into the ribosome. Regulation of the composition of these gonad ribosomes suggests the generation of specialised ribosomes for specific functions.

For the first time we have purified ribosomes from complex *in vivo* tissues. We have solved the cryo-EM structures of three different ribosome complexes; 80S ribosomes from the testis (3.5 Å), 80S ribosomes from the ovary (3.0 Å) and polysomal ribosomes from the testis (4.9 Å), improving the resolution from the only other previous ribosome structure from *D. melanogaster* [29]. One key difference was the testis 80S structure contains the *Drosophila* ortholog of IFRD2. Its presence indicates there is functional homology between CG31694 and IFRD2 in inhibiting mRNA translation through the ribosome, during differentiation. In mammals IFRD2 was seen in differentiating reticulocytes [32], whilst in our work we found CG31694 in the testis 80S (but not in the ovary 80S) where it could be involved in regulation of translation during the differentiation of spermatocytes, which is central to the function of the testis.

The paralogs we find switching in the gonads are localised in three clusters; a) the head of the 40S near the mRNA channel, b) the surface-exposed back of the large subunit and c) ribosome

306 stalks, potentially interacting with the mRNA during translation. The position of these three clusters
307 provides potential explanations of how specialisation is achieved, mechanistically. Differences in
308 amino acid sequence and precise position of the testis and ovary specialised paralogs (Fig 6C-F) can
309 potentially affect the interaction of the mRNA and the ribosome, specifically during initiation when
310 40S ribosomes are recruited to the 5' end of mRNAs. The back of the 60S where RpL22 and RpL22-
311 like are located, would provide an ideal site for additional protein factors to differentially bind to
312 ribosomes containing these proteins. This is particularly true for this paralog pair, which has the
313 lowest sequence identity between each other, 45%. The termini of these proteins are likely to be
314 dynamic given the lack of density for them in our structures. Our phylogenomic analysis suggests
315 that the modulation of this part of the exterior ribosome surface is in common across many
316 organisms, and that the generation of paralogs has occurred independently three times for RpL22.
317 Therefore, this potential mechanism might regulate the ribosome across many eukaryotes. Although
318 paralogs are not conserved across a range of organisms, and many are limited to Drosophilids, there
319 are many organisms with many RP paralog pairs, including human (19 pairs) and *Arabidopsis* (80
320 pairs). Therefore, these potential mechanisms of ribosome regulation could be conserved, if not the
321 precise details.
322 The result we find here, that the gonads are important sites of ribosome heterogeneity and
323 specialisation, further indicates how important mRNA translational regulation is in the testis and
324 ovary. Many other testis-specific translation components exist to enable tight regulation such as
325 eIF4-3 [24] and it is now clear that RP paralog switching also plays a part in this regulation.
326 The importance of the paralog-switching event between RpS5a and Rp5b has recently been
327 functionally characterised in the *Drosophila* ovary [33]. Females without RpS5b produce ovaries with
328 developmental and fertility defects, whilst those without RpS5a have no defects. RpS5b specifically
329 binds to mRNAs encoding proteins with functions enriched for mitochondrial and metabolic GO
330 terms in the ovary, suggesting ovary RpS5b containing ribosomes translate this specific pool of
331 mRNAs [33]. It will be interesting to see how widespread this finding is for RpS5b, since this is a
332 frequently switched paralog: we find that 50% of ovary 80S ribosomes contain RpS5b, whilst 45% of
333 embryo 80S and 30% of testis 80S also contain RpS5b. It has been known for some time that
334 mutations in RpS5a produce a *Minute* phenotype (including infertility), so it seems likely that these
335 two paralogs both have biologically important roles in the fly. RpS5a and RpS5b have also been seen
336 to exhibit tissue-specific expression in *A. thaliana*, in a developmentally regulated manner[13].
337 atRpS5a was suggested to be more important than atRpS5b during differentiation, because of its
338 expression pattern, but the regulation mechanism remains elusive in *A. thaliana*.
339 The function of the RpL22 and RpL22-like paralog pair in *Drosophila* testis has been explored
340 and it has been suggested that the two proteins are not functionally redundant in development or
341 spermatogenesis. However, knockdown of RpL22 is partially rescued by RpL22-like and vice versa
342 [34, 35]. Further work is needed to directly link effects on ribosome composition and mRNA
343 translational output, as the two paralogs may interact with different pools of mRNA in the
344 testis [35].
345 Interestingly, we found little differences between 80S and polysomal ribosome composition
346 apart from an enrichment of RpL24-like and RpL7-like in 80S ribosomes in the ovary. RpL24-like is
347 thought to have a role in the formation and processing pre-60S complexes (by similarity), with RpL24
348 replacing RpL24-like at the very end of processing [36]. Given that we saw enrichment of RpL24-like
349 in 80S compared to polysomes in the ovary, it suggests that a proportion of these 80S complexes
350 could represent the final stage of testing 80S competency in the ovaries. It is not clear why this
351 would be the case in the ovary and not in other tissues. RpL24-like is present in other insects and
352 some non-insect arthropods (FlyBase). A paralog switching event between RpL24 and RpL24-like
353 could be important in translation initiation or indeed provide a platform for additional proteins to
354 bind to the ribosome, given RpL24/RpL24-like is located close to RpL22/RpL22-like.
355 Several of the RPs that have gonad specific paralog pairs (including RpS19, RpS5, RpS10, RpS28
356 and RpL22 [37, 38]) have been linked with human diseases, specifically Diamond-Blackfan anemia

357 and cancer (Table 2). Thus, it will be important to uncover their contribution to mRNA translation
358 regulation and work *in vivo* using *Drosophila* could help understand how they contribute to the
359 translation of specific mRNAs.
360 One of the few canonical RPs we found to be differentially incorporated was RpS11 in the head
361 80S ribosomes. RpS11 phosphorylation, in humans, has been found to be linked to Parkinson's
362 disease [39] and higher levels of RpS11 correlate with poorer prognosis in glioblastoma patients [40].
363 Therefore, understanding RpS11 levels in *Drosophila* head could provide a mechanism of future
364 exploration for dissecting the molecular mechanisms by which RP mutations result in human
365 disease.
366 Altogether our data reveal ribosome heterogeneity occurs in a tissue specific manner. Paralog-
367 switching events are most abundant in the gonads and our structural analysis has provided insights
368 into how this switch might regulate translation mechanistically. Additionally, our evolutionary data
369 suggest specialisation may represent a conserved mechanism of translation regulation across
370 eukaryotes.
371
372 Materials and Methods
373
374 **Growth conditions**
375 *Drosophila melanogaster* wild type (Dahomey) were raised on standard sugar–yeast agar (SYA) [41] .
376 Flies were kept at 25°C and 50% humidity with a 12:12 hr light:dark cycle in 6 oz Square Bottom
377 Bottles (Flystuff). Semi-adherent S2 cells were maintained in Schneider's medium containing L-
378 glutamine (Sigma) supplemented with 10% FBS (Sigma), 100 U/mL penicillin, 100 µg/mL
379 streptomycin, 25 µg/mL amphotericin B (GE Healthcare) and maintained at 26°C in non-vented,
380 adherent flasks (Sarstedt).
381
382 **Tissue harvest**
383 ~300 pairs of ovaries were harvested from 3-6 day old females in 1X PBS (Lonza) with 1 mM DTT
384 (Sigma) and 1 U/µL RNAsin Plus (Promega) and flash frozen in liquid nitrogen. ~500 (rep 1) and
385 ~1000 (rep 2) pairs of testes were harvested from 1-4 day old males in 1X PBS with 4 mM DTT and 1
386 U/µL RNAsin Plus and flash frozen in groups of ~10 pairs. ~500 heads (50:50 female:male, 0-4 days
387 old) per gradient were isolated by flash freezing whole flies and subjecting them to mechanical shock
388 to detach heads. Heads were passed through 1 mm mesh filter with liquid nitrogen and transferred
389 to Dounce homogeniser for lysis. ~500 µL of 0-2 hour embryos/gradient were obtained from cages
390 after pre-clearing for 2 hours. Laying plates comprised of 3.3% agar, 37.5% medium red grape juice
391 compound (Young's Brew) and 0.3% methyl 4-hydroxybenzoate, supplemented with yeast paste of
392 active dried yeast (DCL) and dH20. Embryos were washed in dH20 and embryo wash buffer
393 (102.5 mM NaCl (Sigma), 0.04% TritonX-100 (Sigma) and then flash frozen with minimal liquid. ~120
394 $x10^6$ cells/gradient were treated with 100 µg/mL cycloheximide (Sigma) for 3 minutes before
395 harvesting. Cells were pelleted at 800 xg for 8 minutes, washed in ice-cold 1X PBS supplemented
396 with 100 µg/mL cycloheximide.
397
398 **Ribosome purification**
399 All stages were performed on ice or at 4°C wherever possible. Ovaries and testes were
400 disrupted using RNase-free 1.5mL pestles (SLS) in lysis buffer A (50 mM Tris-HCl pH 8 (Sigma),
401 150 mM NaCl, 10 mM $MgCl_2$ (Fluka), 1% IGEPAL CA-630 (Sigma), 1 mM DTT, 100 µg/mL
402 cycloheximide, 2 U/µL Turbo DNase (Thermo Fisher), 0.2 U/µL RNasin Plus, 1X EDTA-free protease
403 inhibitor cocktail (Roche)). Ovaries, testes and S2 cells were lysed in 500 µL lysis buffer A. Heads
404 were lysed using 8 mL Dounce homogeniser with loose pestle in 1.5mL lysis buffer B (10 mM Tris-HCl
405 pH 7.5 (Gibco), 150 mM NaCl, 10 mM MgCl2, 1% IGEPAL CA-630, 1% Triton X-100, 0.5% sodium
406 deoxycholate (Sigma), 2 mM DTT, 200 µg/mL cycloheximide, 2 U/µL Turbo DNase, 40 U/mL RNAsin
407 Plus, 1X EDTA-free protease inhibitor cocktail). Then 500 µL aliquots were transferred to 2 ml

408 Dounce with tight pestle and further lysed for approximately 30 strokes. Embryos were ground in
409 liquid nitrogen using pestle and mortar and added to lysis buffer B. All lysates were lysed for ≥30
410 mins with occasional agitation, then centrifuged for 5 minutes at 17,000 xg to remove nuclei. Head
411 and embryo cytoplasmic supernatants were obtained by avoiding both floating fat and insoluble
412 pellet and repeatedly centrifuged until free of debris.
413 Cytoplasmic lysates were loaded onto 18 – 60% sucrose gradients (50mM Tris-HCl pH 8.0,
414 150 mM NaCl, 10 mM $MgCl_2$, 100 µg/mL cycloheximide, 1 mM DTT, 1X EDTA-free protease inhibitor
415 cocktail) and ultra-centrifuged in SW40Ti rotor (Beckman) for 3.5 h at 170,920 xg at 4°C. Fractions
416 were collected using a Gradient Station (Biocomp) equipped with a fraction collector (Gilson) and
417 Econo UV monitor (BioRad). Fractions containing 80S were combined, and same with polysomes.
418 Fractions were concentrated using 30 kDa column (Amicon Ultra-4 or Ultra-15) at 4°C and buffer
419 exchanged (50 mM Tris-HCl pH 8, 150 mM NaCl, 10 mM $MgCl_2$) until final sucrose ≥0.1%. Samples
420 were quantified using Qubit Protein Assay Kit.
421
422 **TMT mass spectrometry**
423 40 µg purified protein per sample was subject to tandem mass tag mass spectrometry using Orbitrap
424 Fusion Mass Spec machine by University of Bristol Proteomics Facility. Sequest search was
425 performed against the UniProt *Drosophila* database plus 'Common Contaminants' database and
426 filtered using a 5% FDR cut-off [42].
427
428 **TMT analysis**
429 To be confident of protein identity and presence results were filtered to only include protein IDs
430 where 30% of each protein was covered my mass spec peptides and based on 2 or more unique
431 peptide identities. Only peptide IDs corresponding to *D. melanogaster* proteins were considered. For
432 TMT1 this resulted in a list of 836 proteins and TMT 2, 836 proteins. The full list of *D. melanogaster*
433 ribosomal proteins was extracted from FlyBase (April 2019). Abundances are the sum of the S/N
434 values for the TMT reporter groups for all PSMs matched to the protein. Normalised abundances of
435 these values are then normalised to Total Peptide Amount in each sample such that the total signal
436 from each TMT tag is the same. Normalised abundances were used to quantify levels of proteins. To
437 quantify relative incorporation of paralogs into ribosomes normalised abundances were used to
438 generate percentages, assuming the sum of paralog 1 and paralog 2 were 100%. Several paralogs
439 were not detected and therefore calculated to be 0%, several failed to pass our standard thresholds
440 but were included in this analysis for completeness. Analysis of TMT data and hierarchical clustering
441 was performed in R.
442
443 **Source of RNA-Seq data**
444 RNA-Seq data was extracted from ModMine (intermine.modencode.org) with data from
445 modENCODE project.
446
447 **Cryo-EM**
448 For cryo-EM, 400 mesh copper grids with a supporting carbon lacey film coated with an ultra-thin
449 carbon support film < 3 nm thick (Agar Scientific, UK) were employed. Grids were glow-
450 discharged for 30 seconds (easiGlow, Ted Pella) prior to applying 3 µL of purified ribosomes, and
451 vitrification was performed by plunge-freezing in liquid ethane cooled by liquid nitrogen using a
452 Leica EM GP device (Leica Microsystems). Samples were diluted using the buffer exchange buffer
453 (50 mM Tris pH 8, 150 mM NaCl, 10 mM $MgCl_2$) as required. Cryo-EM data was collected on a FEI
454 Titan Krios (Astbury Biostructure Laboratory, University of Leeds) EM at 300 kV, using a total
455 electron dose of 80 $e^-/Å^2$ and a magnification of 75,000 × at -2 to -4 µm defocus. Movies were
456 recorded using the EPU automated acquisition software on a FEI Falcon III direct electron
457 detector, with a final pixel size of 1.065 Å/pixel (Sup Table 1).
458

459 **Image processing**

460 Initial pre-processing and on-the-fly analysis of data was performed as previously described [43].
461 Image processing was carried out using RELION 2.0/2.1 or 3.0 [44]. MOTIONCOR2 [45] was used
462 to correct for beam-induced motion and calculate averages of each movie. gCTF [46] was used to
463 contrast transfer function determination. Particles were automatically picked using the Laplacian
464 of Gaussian function from RELION [47]. Particles were classified using a reference-free 2D
465 classification. Particles contributing to the best 2D class averages were then used to generate an
466 initial 3D model. This 3D model was used for 3D classification, and the best 3D classes/class were
467 3D refined, followed by per-particle CTF correction and Bayesian polishing [47]. Post-processing
468 was employed to mask the model, and to estimate and correct for the B-factor of the maps [48].
469 The testis 80S map was further processed by multi-body refinement, as previously described [49].
470 The final resolutions were determined using the 'gold standard' Fourier shell correlation
471 (FSC = 0.143) criterion (Sup Table 1). Local resolution was estimated using the local resolution
472 feature in RELION.
473
474 **Atomic modelling**

475 *D. melanogaster* embryo ribosome (pdb code 4v6w) was used as a model to calculate the
476 structures of the testis and ovary ribosomes. First, the full atomic model was fitted into the testis
477 80S cryo-EM average using the 'fit in map' tool from Chimera [50]. Then, fitting was refined by
478 rigid-body fitting individual protein and RNA pdbs into the maps using Chimera. The 18S and 28S
479 ribosomal RNAs were split into two separate rigid bodies each. Proteins and RNAs not present in
480 our averages (i.e. elongation factor 2 and Vig2 for all models, and E-tRNA for the 80S ribosome
481 models) and proteins and RNA with poor densities (i.e. RpLP0 and RpL12, and some regions of the
482 18S and 28S ribosomal RNAs) were removed at this stage. The paralog proteins used for each
483 ribosome are listed in Table 1. For the testis 80S atomic model, CG31694-PA was modelled using
484 SWISS-MODEL [51]. For the testis polysome model, the mRNA was based on pdb model 6HCJ, and
485 the E-tRNA on pdb model 4V6W. The full atomic models were refined using Phenix [52], and the
486 paralogs listed in Fig 2A were manually inspected and corrected using COOT [53] (except Rp10Ab,
487 which was not manually inspected due to the low resolution of that area in the average maps, and
488 RpLP0, which was not present in the model). This cycle was repeated at least three times per
489 ribosome model. The quality of the atomic models was assessed using the validation server from the
490 pdb website (https://validate-pdbe.wwpdb.org/). As the 60S acidic ribosomal protein P0 deposited
491 in the pdb (4v6w) is from *Homo sapiens*, we generated a homology model using SWISS-MODEL. This
492 protein was rigid-body fitted using Chimera after the atomic model refinement and is displayed in
493 Fig 5 for relative position and size comparison purposes only. Figures were generated using Chimera.
494
495 **Vertebrate dataset construction**

496 Coding DNA sequence (CDS) data for 207 vertebrate animals and 4 non-vertebrates (*D.*
497 *melanogaster*, two *Caenorhabditis* species and *S. cerevisiae*) was obtained from Ensembl (release 97,
498 [54]). We performed homology searches using two human Rpl22 family proteins (RPL22 and RPL22L)
499 were searched against 6,922,005 protein sequences using BLASTp (e^{-5}) [55]. We identified 1,082
500 potential RpL22 proteins from 185 vertebrates and 4 non-vertebrates, which were homologous to
501 one or both human RpL22 proteins. As an initial step to reduce the amount of redundancy in the
502 vertebrate dataset, 181 potential RpL22 proteins from 42 selected vertebrates (including humans)
503 were retained to represent as broad a taxonomic sampling of the group. All non-vertebrate
504 sequences, with the exception of two *S. cerevisiae* Rpl22 proteins (RPL22A and RPL22B), were also
505 removed from the dataset. 92 alternative transcripts and spurious hits were removed from the
506 dataset through manual cross-validation with Ensembl Genome Browser to give total of 87
507 vertebrate and 2 yeast RpL22 family proteins.
508
509

510 **Invertebrate dataset construction**

511 CDS data data for 78 invertebrate animals was obtained from Ensembl Metazoa (release 44,
512 [54]). The sequence homology search was performed using two *D. melanogaster* Rpl22 family
513 proteins (RPL22 and RPL22-like) were searched against 1,618,385 protein sequences using BLASTp
514 (e^{-5}) [55]. BLASTp identified 90 potential Rpl22 family proteins across 70 invertebrates, which were
515 homologous to one or both *D. melanogaster* Rpl22 proteins. 15 alternative transcripts and spurious
516 hits were removed from the dataset through manual cross-validation with Ensembl Genome
517 Browser to give total of 75 invertebrate RpL22 family proteins. Together with 87 vertebrate and 2
518 outgroup proteins, our final dataset consisted of 164 RpL22 family proteins sampled across the
519 metazoan tree of life.
520

521 **Phylogenetic reconstructions of metazoan RpL22 family**

522 Initial phylogenetic reconstruction of the metazoan RpL22 family was performed using the
523 full dataset of 164 sequences (87 invertebrate sequences, 75 vertebrate sequences and two yeast
524 sequences). All sequences were aligned using three different alignment algorithms: MUSCLE [56],
525 MAFFT [57] and PRANK [58]. MUSCLE was run with the default parameters, and MAFFT was run with
526 the automatically-selected most-appropriate alignment strategy (in this case, L-INS-I). PRANK was
527 run with both the default parameters and the PRANK+F method with "permanent" insertions. All
528 four resultant alignments were compared against each other using MetAl [59], and were all judged
529 to be mutually discordant based on differences of 20-25% between each pair of alignments. Column-
530 based similarity scores were calculated for each alignment using the norMD statistic [60]. The
531 MUSCLE alignment had the highest column-based similarity score (1.281) and was selected for
532 further analysis. This alignment was trimmed using TrimAl's gappyout method [61]. Maximum-
533 likelihood phylogenetic reconstruction was performed on the trimmed alignment using IQTREE [62],
534 with a WAG+R6 model selected by ModelFinder Plus [63] and 100 bootstrap replicates.
535 A reduced sampling of the metazoan Rpl22 family was used to generate a phylogeny was
536 performed using taxonomically-representative dataset containing 50 Rpl22 genes from 30 animals
537 and *S. cerevisiae*. This dataset was aligned using the same four methods described above, and all
538 alignments were judged to be mutually discordant (differences of 19-37%) using MetAl [59]. The
539 MUSCLE alignment had the highest column-based similarity score assigned by norMD (0.702) and
540 was selected for further analysis. As above, this alignment was trimmed using TrimAl's gappyout
541 method. Maximum-likelihood phylogenetic reconstruction was performed on the trimmed
542 alignment using IQTREE [62], with a DCMut+R3 model selected by ModelFinder Plus [63] and 100
543 bootstrap replicates.
544

545 **Data deposition**

546 The EM-density maps for testis 80S, testis polysomes and ovaries 80S are deposited in the EMDB
547 under the accession numbers EMD-10622, EMD-10623 and EMD-10624. The refined models are
548 deposited in the PDB under accession codes 6XU7, pdb 6XU7 and pdb 6XU8.
549

550 **Acknowledgements**

551 We thank the Astbury Biostructure Laboratory (ABSL) Facility Staff for assisting with cryo-EM data
552 collection. All Electron Microscopy was performed at ABSL which was funded by the University of
553 Leeds and the Wellcome Trust (108466/Z/15/Z). Electron microscopy image processing was
554 partially undertaken on ARC3, part of the High Performance Computing (HPC) facilities at the
555 University of Leeds. CGPM and MJOC would like to thank The University of Nottingham for HPC
556 facilities and staffing. Mass spectrometry was performed by Bristol University Proteomics Facility.
557 Julie Aspden and Juan Fontana are funded by the University of Leeds (University Academic Fellow
558 scheme). This work was funded by Royal Society (RSG\R1\180102), BBSRC (BB/S007407/1),
559 Wellcome Trust ISSF (105615/Z/14/Z), White Rose University Consortium- Collaborative Grant
560 and MRC (MR/N000471/1). MA was funded from BBSRC DTP BB/M011151/1.

561
562 **References**

563 1. Kondrashov, N., et al., *Ribosome-mediated specificity in Hox mRNA translation and*
564 *vertebrate tissue patterning.* Cell, 2011. **145**(3): p. 383-97.
565 2. Shi, Z., et al., *Heterogeneous Ribosomes Preferentially Translate Distinct Subpools of mRNAs*
566 *Genome-wide.* Molecular Cell, 2017.
567 3. Segev, N. and J.E. Gerst, *Specialized ribosomes and specific ribosomal protein paralogs*
568 *control translation of mitochondrial proteins.* J Cell Biol, 2018. **217**(1): p. 117-126.
569 4. García-Marcos, A., et al., *Yeast ribosomal stalk heterogeneity in vivo shown by two-photon*
570 *FCS and molecular brightness analysis.* Biophys J, 2008. **94**(7): p. 2884-90.
571 5. Bortoluzzi, S., et al., *Differential expression of genes coding for ribosomal proteins in*
572 *different human tissues.* Bioinformatics, 2001. **17**(12): p. 1152-7.
573 6. Simsek, D., et al., *The Mammalian Ribo-interactome Reveals Ribosome Functional Diversity*
574 *and Heterogeneity.* Cell, 2017. **169**(6): p. 1051-1065 e18.
575 7. Kearse, M.G., A.S. Chen, and V.C. Ware, *Expression of ribosomal protein L22e family*
576 *members in Drosophila melanogaster: rpL22-like is differentially expressed and alternatively*
577 *spliced.* Nucleic Acids Res, 2011. **39**(7): p. 2701-16.
578 8. Carroll, A.J., et al., *Analysis of the Arabidopsis cytosolic ribosome proteome provides detailed*
579 *insights into its components and their post-translational modification.* Mol Cell Proteomics,
580 2008. **7**(2): p. 347-69.
581 9. Natchiar, S.K., et al., *Visualization of chemical modifications in the human 80S ribosome*
582 *structure.* Nature, 2017. **551**(7681): p. 472-477.
583 10. Dinman, J.D., *Pathways to Specialized Ribosomes: The Brussels Lecture.* J Mol Biol, 2016.
584 **428**(10 Pt B): p. 2186-94.
585 11. Guimaraes, J.C. and M. Zavolan, *Patterns of ribosomal protein expression specify normal and*
586 *malignant human cells.* Genome Biol, 2016. **17**(1): p. 236.
587 12. Szakonyi, D. and M.E. Byrne, *Ribosomal protein L27a is required for growth and patterning in*
588 *Arabidopsis thaliana.* Plant J, 2011. **65**(2): p. 269-81.
589 13. Weijers, D., et al., *An Arabidopsis Minute-like phenotype caused by a semi-dominant*
590 *mutation in a RIBOSOMAL PROTEIN S5 gene.* Development, 2001. **128**(21): p. 4289-99.
591 14. Marygold, S.J., C.M. Coelho, and S.J. Leevers, *Genetic analysis of RpL38 and RpL5, two*
592 *minute genes located in the centric heterochromatin of chromosome 2 of Drosophila*
593 *melanogaster.* Genetics, 2005. **169**(2): p. 683-95.
594 15. Thurmond, J., et al., *FlyBase 2.0: the next generation.* Nucleic Acids Res, 2019. **47**(D1): p.
595 D759-D765.
596 16. Barakat, A., et al., *The organization of cytoplasmic ribosomal protein genes in the*
597 *Arabidopsis genome.* Plant Physiol, 2001. **127**(2): p. 398-415.
598 17. Richter, J.D. and P. Lasko, *Translational control in oocyte development.* Cold Spring Harb
599 Perspect Biol, 2011. **3**(9): p. a002758.
600 18. Qin, X., et al., *Global analyses of mRNA translational control during early Drosophila*
601 *embryogenesis.* Genome Biol, 2007. **8**(4): p. R63.
602 19. Boria, I., et al., *The ribosomal basis of Diamond-Blackfan Anemia: mutation and database*
603 *update.* Hum Mutat, 2010. **31**(12): p. 1269-79.
604 20. Slaidina, M. and R. Lehmann, *Translational control in germline stem cell development.* J Cell
605 Biol, 2014. **207**(1): p. 13-21.
606 21. Yu, J., et al., *Protein synthesis and degradation are essential to regulate germline stem cell*
607 *homeostasis in Drosophila testes.* Development, 2016. **143**(16): p. 2930-45.
608 22. Brengues, M., L. Pintard, and B. Lapeyre, *mRNA decay is rapidly induced after spore*
609 *germination of Saccharomyces cerevisiae.* J Biol Chem, 2002. **277**(43): p. 40505-12.
610 23. Vedelek, V., et al., *Analysis of Drosophila melanogaster testis transcriptome.* BMC Genomics,
611 2018. **19**(1): p. 697.

612 24. Ghosh, S. and P. Lasko, *Loss-of-function analysis reveals distinct requirements of the*
613 *translation initiation factors eIF4E, eIF4E-3, eIF4G and eIF4G2 in Drosophila*
614 *spermatogenesis.* PLoS One, 2015. **10**(4): p. e0122519.
615 25. Lambertsson, A., *The minute genes in Drosophila and their molecular functions.* Adv Genet,
616 1998. **38**: p. 69-134.
617 26. Kongsuwan, K., et al., *A Drosophila Minute gene encodes a ribosomal protein.* Nature, 1985.
618 **317**(6037): p. 555-8.
619 27. Marygold, S.J., et al., *The ribosomal protein genes and Minute loci of Drosophila*
620 *melanogaster.* Genome Biol, 2007. **8**(10): p. R216.
621 28. Martinez Barrio, A., et al., *Targeted resequencing and analysis of the Diamond-Blackfan*
622 *anemia disease locus RPS19.* PLoS One, 2009. **4**(7): p. e6172.
623 29. Anger, A.M., et al., *Structures of the human and Drosophila 80S ribosome.* Nature, 2013.
624 **497**(7447): p. 80-5.
625 30. Heyer, E.E. and M.J. Moore, *Redefining the Translational Status of 80S Monosomes.* Cell,
626 2016. **164**(4): p. 757-69.
627 31. Branco-Price, C., et al., *Genome-wide analysis of transcript abundance and translation in*
628 *Arabidopsis seedlings subjected to oxygen deprivation.* Ann Bot, 2005. **96**(4): p. 647-60.
629 32. Brown, A., et al., *Structures of translationally inactive mammalian ribosomes.* Elife, 2018. **7**.
630 33. Kong, J., et al., *A ribosomal protein S5 isoform is essential for oogenesis and interacts with*
631 *distinct RNAs in Drosophila melanogaster.* Sci Rep, 2019. **9**(1): p. 13779.
632 34. Mageeney, C.M., et al., *Functional interplay between ribosomal protein paralogues in the*
633 *eRpL22 family in Drosophila melanogaster.* Fly (Austin), 2018. **12**(3-4): p. 143-163.
634 35. Mageeney, C.M. and V.C. Ware, *Specialized eRpL22 paralogue-specific ribosomes regulate*
635 *specific mRNA translation in spermatogenesis in.* Mol Biol Cell, 2019. **30**(17): p. 2240-2253.
636 36. Saveanu, C., et al., *Sequential protein association with nascent 60S ribosomal particles.* Mol
637 Cell Biol, 2003. **23**(13): p. 4449-60.
638 37. Campagnoli, M.F., et al., *RPS19 mutations in patients with Diamond-Blackfan anemia.* Hum
639 Mutat, 2008. **29**(7): p. 911-20.
640 38. Cao, B., et al., *Cancer-mutated ribosome protein L22 (RPL22/eL22) suppresses cancer cell*
641 *survival by blocking p53-MDM2 circuit.* Oncotarget, 2017. **8**(53): p. 90651-90661.
642 39. Martin, I., V.L. Dawson, and T.M. Dawson, *Recent advances in the genetics of Parkinson's*
643 *disease.* Annu Rev Genomics Hum Genet, 2011. **12**: p. 301-25.
644 40. Yong, W.H., et al., *Ribosomal Proteins RPS11 and RPS20, Two Stress-Response Markers of*
645 *Glioblastoma Stem Cells, Are Novel Predictors of Poor Prognosis in Glioblastoma Patients.*
646 PLoS One, 2015. **10**(10): p. e0141334.
647 41. Bass, T.M., et al., *Optimization of dietary restriction protocols in Drosophila.* J Gerontol A Biol
648 Sci Med Sci, 2007. **62**(10): p. 1071-81.
649 42. Consortium, U., *UniProt: a worldwide hub of protein knowledge.* Nucleic Acids Res, 2019.
650 **47**(D1): p. D506-D515.
651 43. Thompson, R.F., et al., *Collection, pre-processing and on-the-fly analysis of data for high-*
652 *resolution, single-particle cryo-electron microscopy.* Nat Protoc, 2019. **14**(1): p. 100-118.
653 44. Fernandez-Leiro, R. and S.H.W. Scheres, *A pipeline approach to single-particle processing in*
654 *RELION.* Acta Crystallogr D Struct Biol, 2017. **73**(Pt 6): p. 496-502.
655 45. Zheng, S.Q., et al., *MotionCor2: anisotropic correction of beam-induced motion for improved*
656 *cryo-electron microscopy.* Nat Methods, 2017. **14**(4): p. 331-332.
657 46. Zhang, K., *Gctf: Real-time CTF determination and correction.* J Struct Biol, 2016. **193**(1): p. 1-
658 12.
659 47. Zivanov, J., et al., *New tools for automated high-resolution cryo-EM structure determination*
660 *in RELION-3.* Elife, 2018. **7**.
661 48. Scheres, S.H. and S. Chen, *Prevention of overfitting in cryo-EM structure determination.* Nat
662 Methods, 2012. **9**(9): p. 853-4.

663 49. Nakane, T., et al., *Characterisation of molecular motions in cryo-EM single-particle data by*
664 *multi-body refinement in RELION.* Elife, 2018. **7**.
665 50. Pettersen, E.F., et al., *UCSF Chimera--a visualization system for exploratory research and*
666 *analysis.* J Comput Chem, 2004. **25**(13): p. 1605-12.
667 51. Waterhouse, A., et al., *SWISS-MODEL: homology modelling of protein structures and*
668 *complexes.* Nucleic Acids Res, 2018. **46**(W1): p. W296-W303.
669 52. Afonine, P.V., et al., *New tools for the analysis and validation of cryo-EM maps and atomic*
670 *models.* Acta Crystallogr D Struct Biol, 2018. **74**(Pt 9): p. 814-840.
671 53. Emsley, P., et al., *Features and development of Coot.* Acta Crystallogr D Biol Crystallogr,
672 2010. **66**(Pt 4): p. 486-501.
673 54. Cunningham, F., et al., *Ensembl 2019.* Nucleic Acids Res, 2019. **47**(D1): p. D745-D751.
674 55. Altschul, S.F., et al., *Basic local alignment search tool.* J Mol Biol, 1990. **215**(3): p. 403-10.
675 56. Edgar, R.C., *MUSCLE: multiple sequence alignment with high accuracy and high throughput.*
676 Nucleic Acids Res, 2004. **32**(5): p. 1792-7.
677 57. Katoh, K. and D.M. Standley, *MAFFT multiple sequence alignment software version 7:*
678 *improvements in performance and usability.* Mol Biol Evol, 2013. **30**(4): p. 772-80.
679 58. Loytynoja, A., *Phylogeny-aware alignment with PRANK.* Methods Mol Biol, 2014. **1079**: p.
680 155-70.
681 59. Blackburne, B.P. and S. Whelan, *Measuring the distance between multiple sequence*
682 *alignments.* Bioinformatics, 2012. **28**(4): p. 495-502.
683 60. Thompson, J.D., et al., *Towards a reliable objective function for multiple sequence*
684 *alignments.* J Mol Biol, 2001. **314**(4): p. 937-51.
685 61. Capella-Gutierrez, S., J.M. Silla-Martinez, and T. Gabaldon, *trimAl: a tool for automated*
686 *alignment trimming in large-scale phylogenetic analyses.* Bioinformatics, 2009. **25**(15): p.
687 1972-3.
688 62. Nguyen, L.T., et al., *IQ-TREE: a fast and effective stochastic algorithm for estimating*
689 *maximum-likelihood phylogenies.* Mol Biol Evol, 2015. **32**(1): p. 268-74.
690 63. Kalyaanamoorthy, S., et al., *ModelFinder: fast model selection for accurate phylogenetic*
691 *estimates.* Nat Methods, 2017. **14**(6): p. 587-589.
692

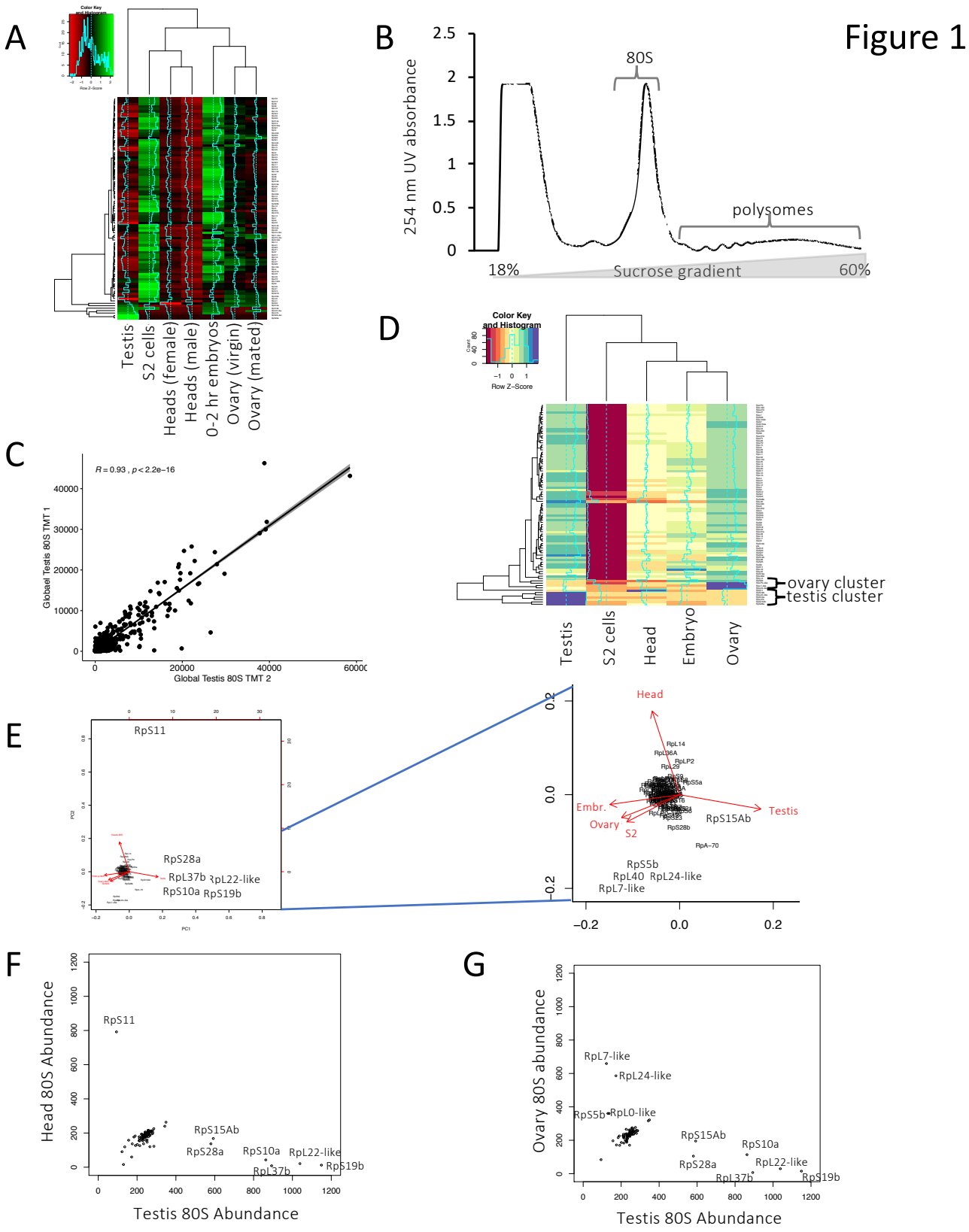

Figure 1: Heterogeneous ribosome populations exist in different tissues
(A) Hierarchical clustering of modENCODE RNA-Seq data for Ribosomal Proteins (RPs) across testis, ovary, head, embryo and S2 cells reveals differences in RP expression. RPKMs are clustered by row. (B) Schematic of strategy used to isolate and compare ribosomal complex composition. (C) Correlation of two biological repeats of TMT mass spec experiment for protein abundances within 80S ribosomes isolated from testis, with Pearson's correlation calculated, shows replicates are reproducible. (D) Identification of heterogeneity of ribosome protein composition across samples. Hierarchical clustering of normalised protein abundances from replicate 2, clustered according to row i.e. ribosomal protein. (E) PCA of RPs, showing most cluster together and behave similarly across tissues. Two groups of proteins are different from majority. (F) Scatter plot of scaled abundances for testis 80S and head 80S for ribosomal proteins. Identification of testis enriched components. Proteins enriched in one sample over the other are labelled. (G) Scatter plot of scaled abundances for testis 80S and ovary 80S for ribosomal proteins. Identification of both testis and ovary enriched components. Proteins enriched in one sample over the other are labelled.

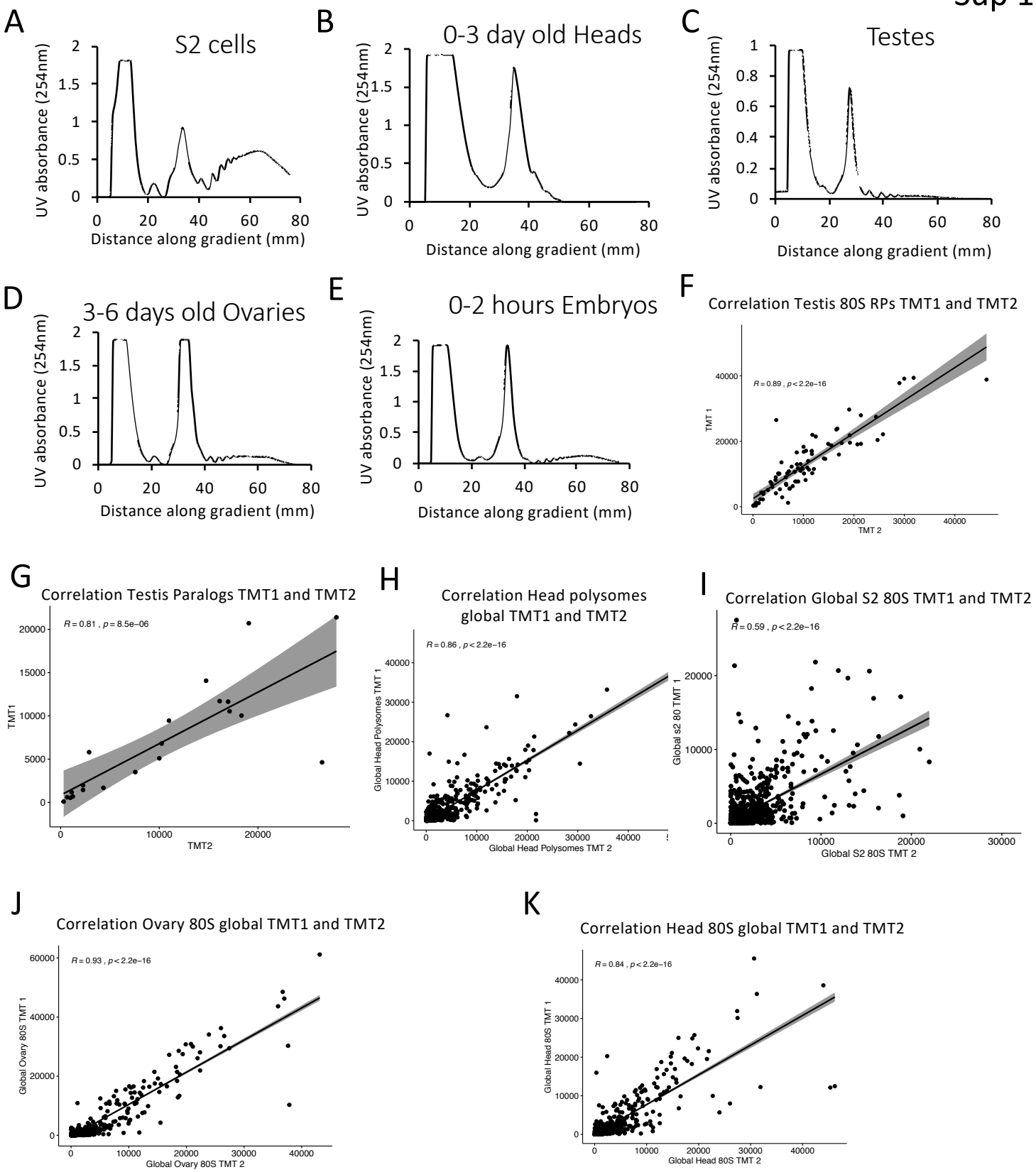

Sup 1: Determined ribosomal composition in tissues and during development

254 nm UV plots across sucrose gradients with 80S and polysomal complexes isolated from (A) S2 cells, (B) 50:50 mixture of female:male 0-3 day old Heads. (C) ~500 pairs of 1-4 day old adult testes, (D) ~500 pairs of 3-6 day old adult ovaries, (E) 0-2 hour embryos. Correlation of two TMT mass spec experiments for protein abundances within 80S ribosomes isolated with Pearson's correlation calculated, shows replicates are reproducible from (F) RPs in testis 80S, (G) RP paralogs in testis 80S, (H) head polysome, (I) S2 80S, (J) ovary 80S, (K) head 80S.

Figure 2

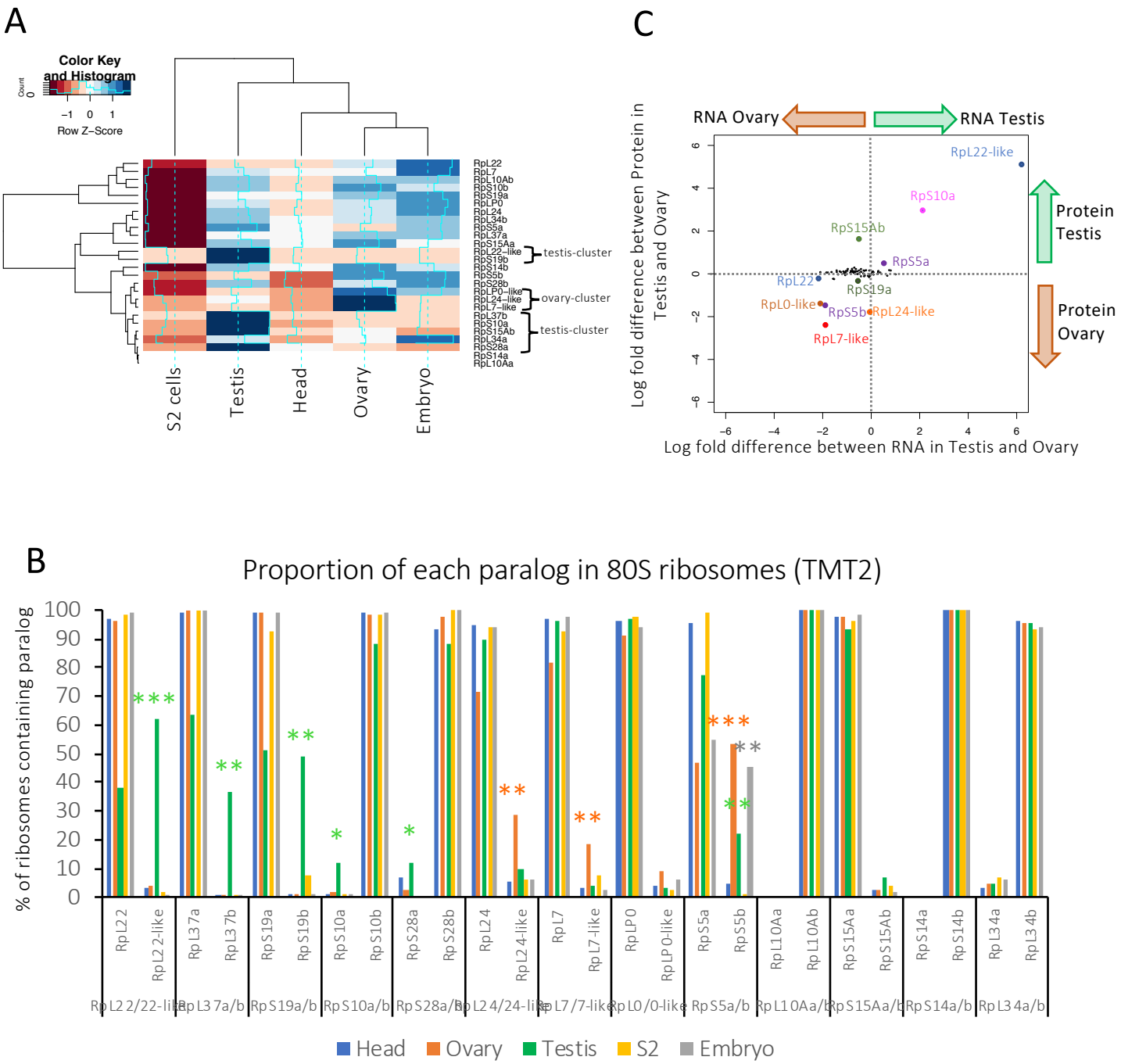

Figure 2: Specialisation of gonad ribosomes through paralog switching
(A) Hierarchical clustering of RP paralog proteins across the 5 samples scaled by row. (B) Proportion of ribosomes containing either of two ribosomal protein paralogs (expressed at percentage). 5 pairs have testis specificity and 4 ovary specificity. *** indicates if second paralog is >50%; with ** if >25% and with * if >10%. (C) Log fold difference plot showing differences between testis and ovary at both RNA (ovary RNA, mated females) and protein levels.

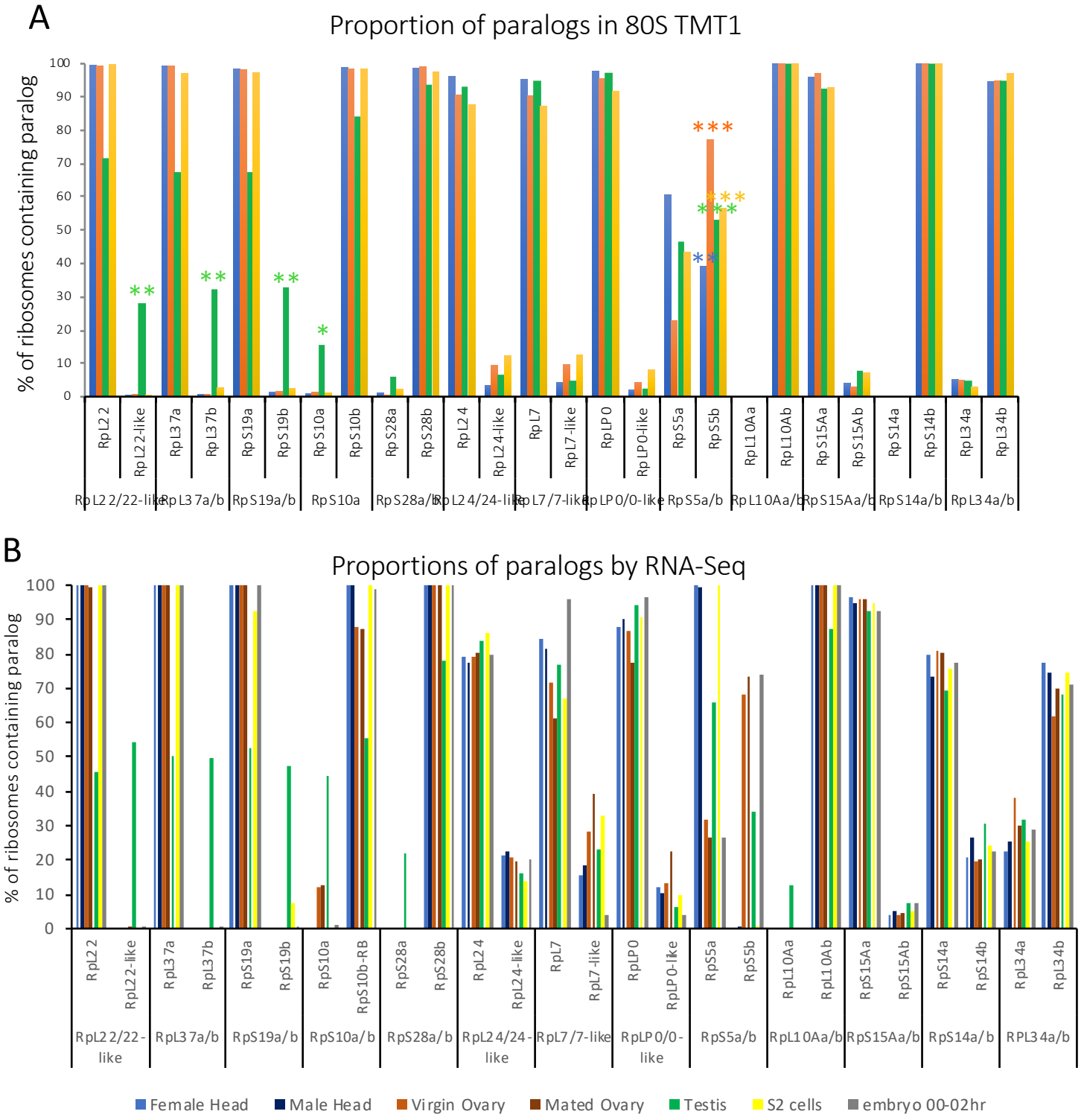

Sup 2: Specialisation of gonad ribosomes through paralog switching

(A) Bar chart of paralog pair % incorporation into 80S ribosomes across different tissues from TMT experiment 1 (head, ovary, testis, S2 cells and 0-2hr embryo). (B) Bar chart of paralog pair % relative expression by ModENCODE RNA-Seq across different tissues (female head, male head, virgin ovary, mated ovary, testis, S2 cells and 0-2hr embryo).

Figure 3

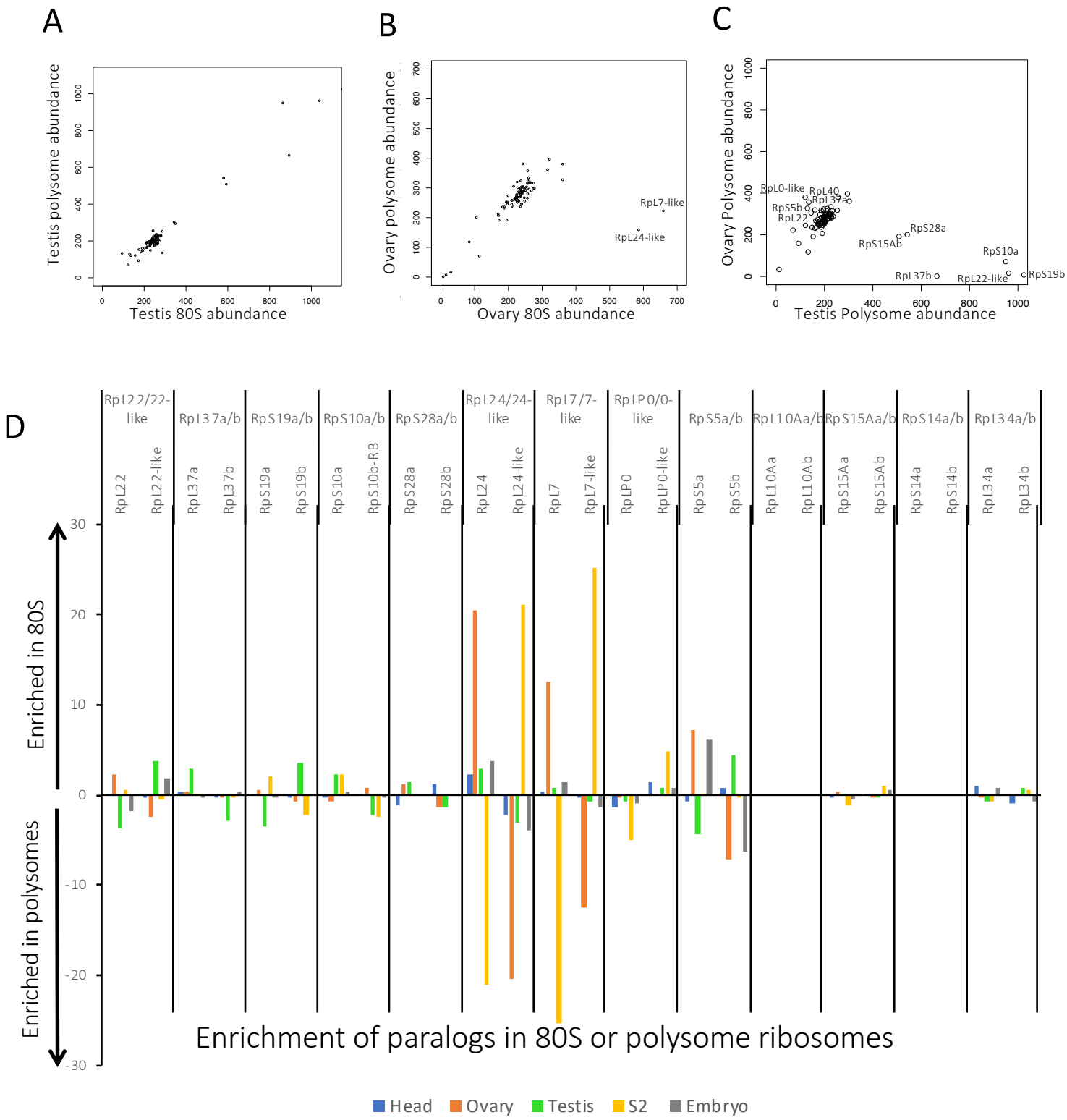

Figure 3: Little difference between composition of 80S and polysome ribosomes
(A) Scatter plot of scaled abundances for testis 80S and testis polysomes for ribosomal proteins shows little difference. (B) Scatter plot of scaled abundances for ovary 80S and ovary polysomes for ribosomal proteins reveals 80S enrichment of RpL7-like and RpL24-like in the 80S. (C) Scatter plot of scaled abundances for testis polysomes and ovary polysomes for ribosomal proteins reveals enrichment of similar proteins differentially incorporated in 80S; Testis RpD15Ab, RpS28a, RpL37b, RpS10a, RpS19b and RpL22-like; Ovary RpL37a, RpL22, RpL40, RpL0-like and RpS5b. (D) Comparison of overall difference in composition between 80S and polysomes across all paralogs and all tissues; showing main difference between 80S and polysome composition is with ovary for RpL24/24-like and RpL7/7-like.

A

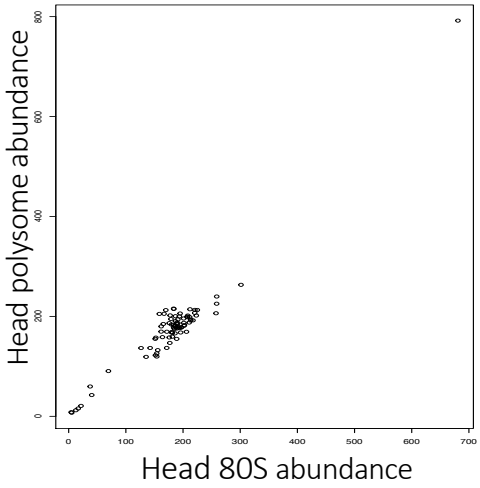

B

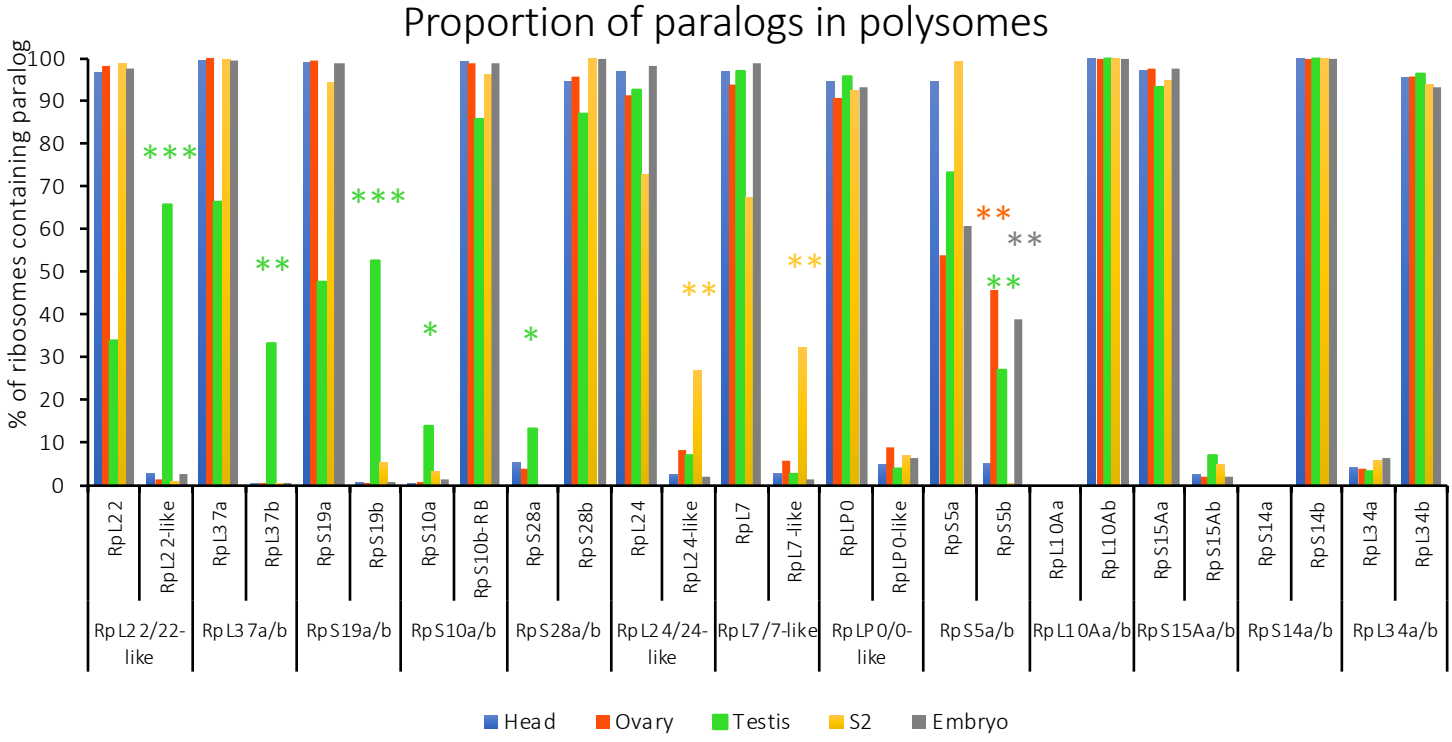

Sup 3: Little difference between composition of 80S and polysome ribosomes
(A) Scatter plot of scaled abundances for head 80S and head polysomes for ribosomal proteins reveals little difference in ribosomes composition. (B) Bar chart of paralog pair % incorporation into polysome ribosomes across different tissues from TMT experiment 2 (head, ovary, testis, S2 cells and 0-2hr embryo).

Figure 4

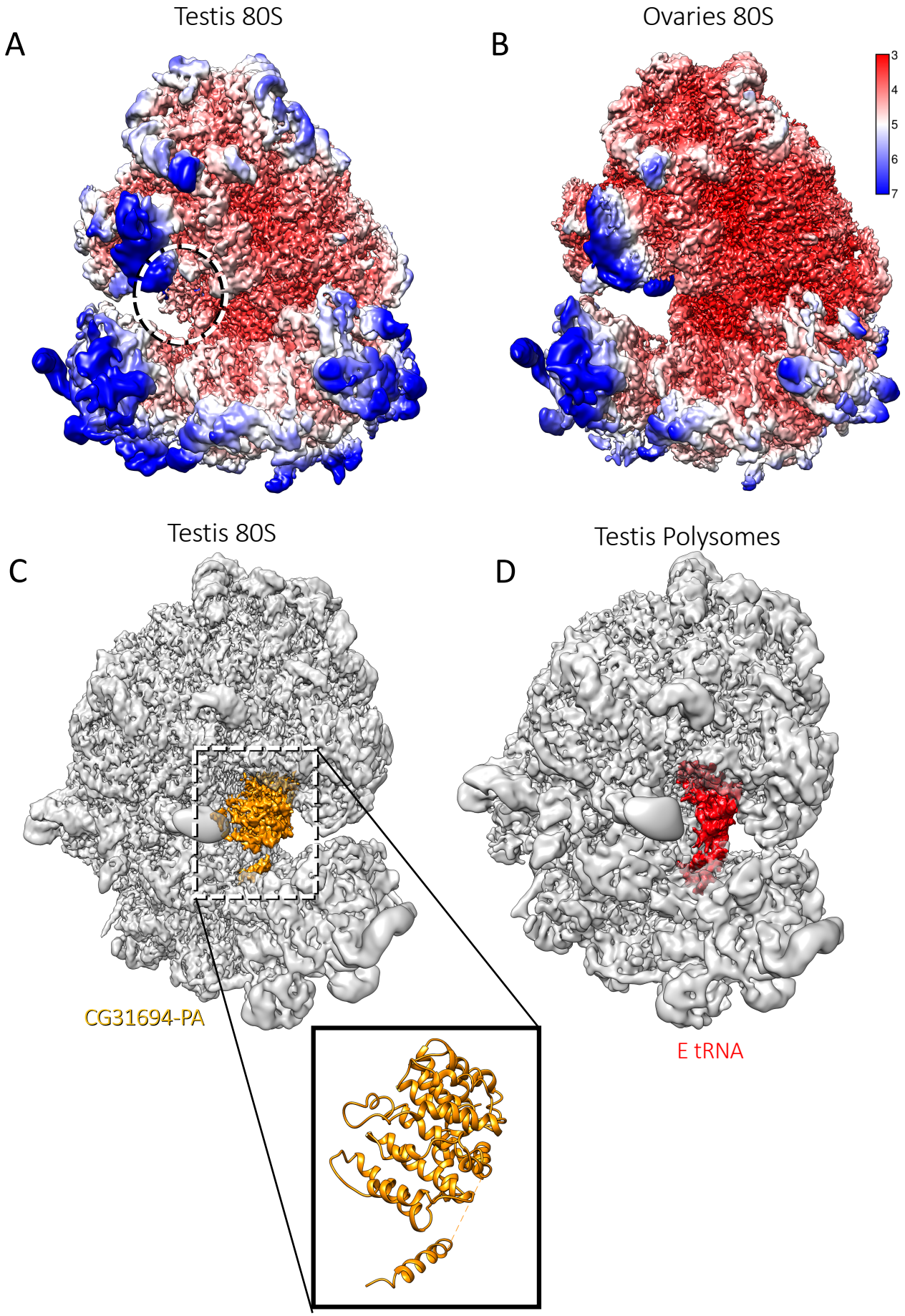

Figure 4: Cryo-electron microscopy of testis and ovary ribosomes
A and B) Electron microscopy averages of testis 80S (A) and ovaries 80S (B) ribosomes, color-coded according to their local resolution. C and D) cryo-EM averages of 80S (C) and polysome (D) ribosomes purified from testes, with segmented densities corresponding to CG31694-PA and E-tRNA colored in orange and red respectively. The atomic model of CG31694-PA is shown in the inset.

Sup 4

A

Testis 80S

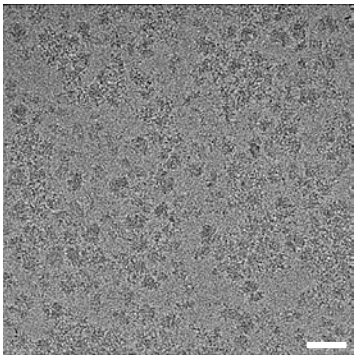

B

Testis 80S resolution = 3.5 Å

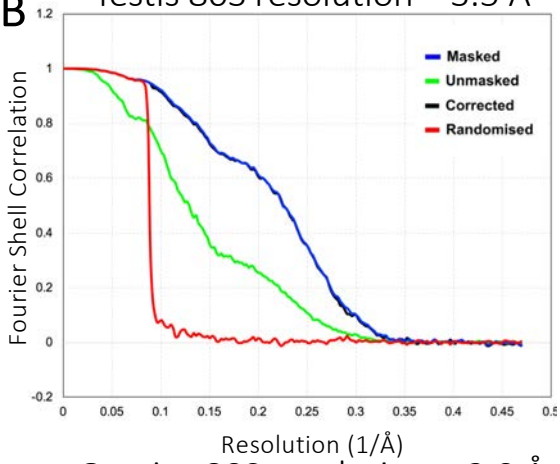

F

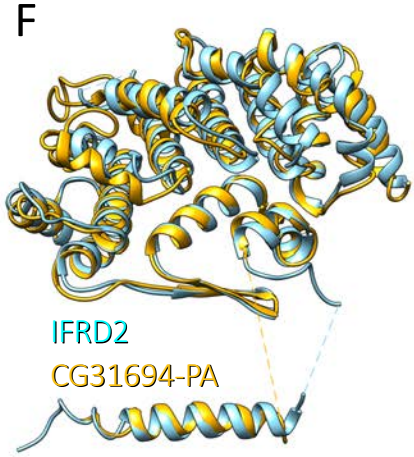

C

Ovaries 80S

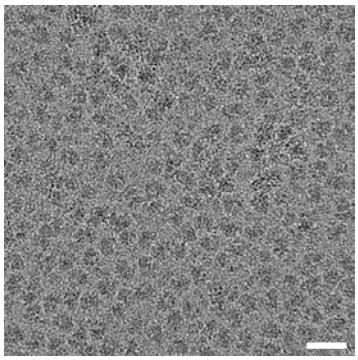

D

Ovaries 80S resolution = 3.0 Å

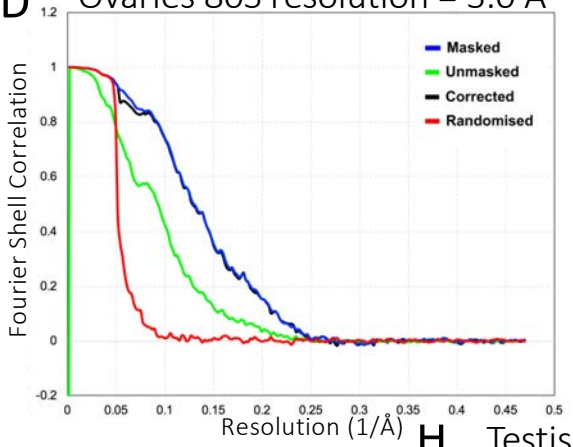

G

Testis Polysomes

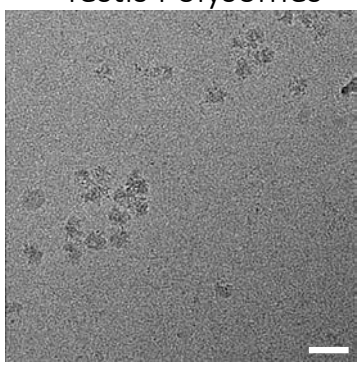

E

```
CLUSTAL O(1.2.4) multiple sequence alignment


CG31694-PA      ------------------------------------------------------------   0
IFRD2           MAWNSPSRRPVWQGGAPREDGGARGVWLPSSGQVSAQRTGRRLVGLEPTPTGSLTPRPPR   60


CG31694-PA      ----MPRRNKKSAAGRG-------RT----NDSN-SEDESFD-NVSVYSHMSEVASSEAT   43
IFRD2           PVPGMPRARKGNTLRKGGQRRGGGARSSAQADSGSSDDEAASEARSTASECPSLLSTTAE.  120
                    *** .* .:  :*              **. *:**: .   *. *.  .: *: *

CG31694-PA      ---------DELANERFEEKFEKALEQATEKSAQTRVQALQAICELLMHRYMPDFVEDRK   94
IFRD2           DSLGGDVVDEQGQQEDLEEKLKEYVDCLTDKSAKTRQGALESLRLALASRLLPDFLLERR.  180
                         ::  :* :***::: ::  *:***:**  **:::   *  * :***: :*:

CG31694-PA      MTLMDFVEKSIRRGKGQEQVWGARLAPLLVLQMGGDE---GISKAMNQFLLNTVQDKSVG   151
IFRD2           LTLADALEKCLKKGKGEEQALAAAVLGLLCVQLGPGPKGEELFHSLQPLLVSVLSDSTAS.  240
                :** * :**.:::***:**. .* :  ** :*:* .     : :::: :*:..:.*.:..

CG31694-PA      FDARAKCCTAVGLLSFLGCEDVGELVHLMQSFEAIFAGSYLRGDDKTPVSVTAEAGTFHA   211
IFRD2           PAARLHCASALGLGCYVAAADIQDLVSCLACLESVFSRFYGLGGSSTSPVVPASLHGLLS   300
                  ** :*.:*:** .::.. *: :**  : .:*::*:  *  *...*   * *.   : :

CG31694-PA      EALNAWGLLLTLIPSGDFVSLMTTGQNMFPSIKKFLGLLQSTHLDVRMAAGETIALILES   271
IFRD2           AALQAWALLLTICPSTQISHILDRQL------PRLPQLLSSESVNLRIAAGETIALLFEL  354
                 **:**.****: ** ::  ::           ::  **.*  :::*:********::*

CG31694-PA      GRAHEEDFLEDDIAELSEAVKQLATDSHKYRAKRDRKAQRATFRDVLRYLEEDISPEISI   331
IFRD2           ARDLEEEFVYEDMEALCSVLRTLATDSNKYRAKADRRRQRSTFRAVLHSVEGGECEEEIV   414
                .*  **:*: :*:  *...:: *****:***** **: **:*** **: :* . . *  :

CG31694-PA      RFGTESLTLDSWSIHHQYSAMCTVMGPGMTSQLQENEFIRDIFQLGPRPTNTGINGNAKV   391
IFRD2           RFGFEVLYMDSWARHRIYAAFKEVLGSGMHHHLQNNELLRDIFGLGPVLLLDATA-LKAC   473
                *** * * :***: *: *:*:  *:* **  :**:**::**** ***     .

CG31694-PA      KPTKLERHLVNAAAFKARSITRGKNRDKRSAVVT   425
IFRD2           KVPRFEKHLYNAAAFKARTKARSRVRDKRADIL-   506
                *  ::*:** ********: :*.: ****: ::
```

H

Testis Polysomes resolution = 4.9 Å

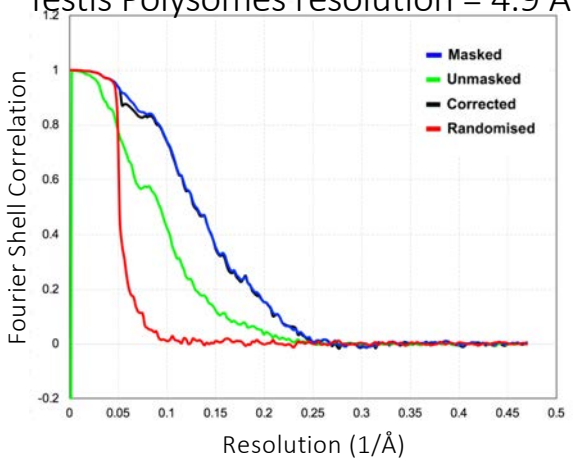

I

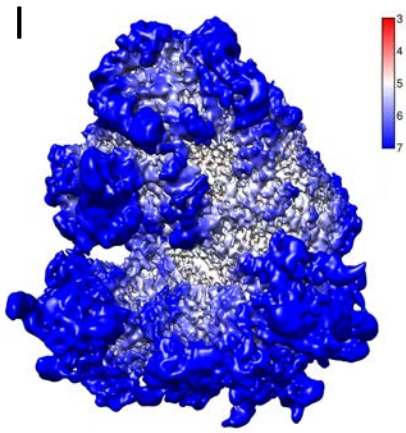

Testis Polysomes

Sup 4: Cryo-electron microscopy of testis and ovaries ribosomes

Cryo-electron micrographs (A, C and G) and FSC curves (B, D and H) for the cryo-EM averages of testis 80S (A & B), ovaries 80S (C & D) and testis polysomes (G & H). (E) Clustal-omega alignment of human, rabbit IRFD2 protein sequence and *D.melanogaster* CG31694-PA protein sequence. (F) Comparison of the atomic models of IFRD2 and CG31694-PA. (I) Electron microscopy average of testis polysomes colour-coded according to its local resolution. Scale bars for A, C & G, 50 nm.

	Testis 80S	Ovary 80S	Testis Polysomes
Data collection			
Microscope	FEI Titan KRIOS	FEI Titan KRIOS	FEI Titan KRIOS
Voltage (keV)	300	300	300
Detector	FEI Falcon III	FEI Falcon III	FEI Falcon III
Magnification	x75,000	x75,000	x75,000
Defocus range	-2 to -4	-2 to -4	-2 to -4
Pixel size (Å)	1.065	1.065	1.065
Electron dose (e^-/Å^2)	80	80	80
Electron dose per frame (e^-/Å^2)	1.35	1.35	1.35
Exposure (sec)	2	2	2
No. of frames	60	60	60
No. of micrographs	5,241	9,076	2,758
Data processing			
Symmetry Point Group	C1	C1	C1
Final particle number	46,878	185,913	10,392
Map average resolution (Å, 0.143 FSC threshold)	3.5	3.0	4.9
Map sharpening B-factor (Å^2)	-150	-118	-197
Multi-body refinement		N/A	N/A
Large subunit			
Map average resolution (Å, 0.143 FSC threshold)	3.5		
Map sharpening B-factor (Å^2)	-143		
Small subunit without head			
Map average resolution (Å, 0.143 FSC threshold)	3.7		
Map sharpening B-factor (Å^2)	-165		
Head of small subunit			
Map average resolution (Å, 0.143 FSC threshold)	4.8		
Map sharpening B-factor (Å^2)	-224		
Refinement			
Initial model (PDB code)	4v6w	Testis 80S model	Testis 80S model
Model Composition			
Non-hydrogen atoms	219,859	217,079	219,021
Amino acid residues	12,106	11,755	11,764
Nucleotides	5,916	5,916	6,003
R.M.S.D. from ideal geometry			
Bond lengths (Å)	0.008	0.011	0.017
Bond angles (º)	1.027	1.315	1.794
Validation			
Clashscore	10.57	7.8	15.56
Rotamer outliers (%)	0.82	1.23	1.90
Ramachandran plot statistics			
Favored (%)	86.50	83.81	82.22
Allowed (%)	13.00	15.31	17.02
Outliers (%)	0.50	0.88	0.76

Sup Table 1: Summary of data collection, image processing, model building, refinement and validation statistics

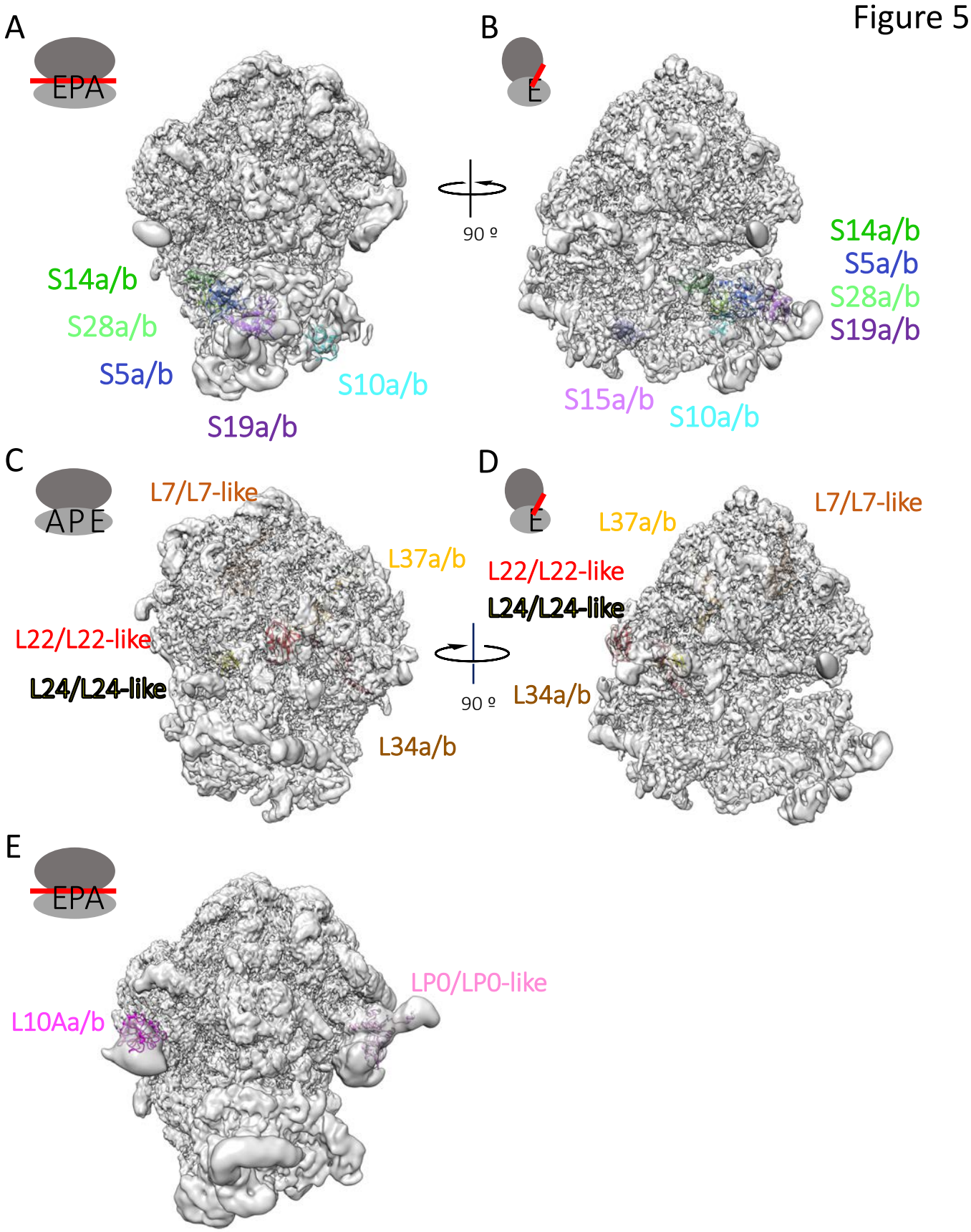

Figure 5: Location of *D. melanogaster* ribosomal paralogs
Ribosomal paralogs were mapped to the testis 80S EM average. (A & B) Small subunit paralogs: RpS14a/b (dark green), RpS28a/b (light green), RpS5a/b (dark blue), RpS19a/b (dark purple), RpS10a/b (cyan) and S15a/b (light purple). Paralogs are shown viewed from the front of ribosome (A) and from the side into mRNA channel (B). (C & D) Large subunit paralogs: L7/L7-like (light brown), L22/L22-like (red), L24/L24-like (yellow), L34a/b (dark brown) and L37a/b (orange). Paralogs are viewed from back of the ribosome (C) and from the side into mRNA channel (D). E) Paralogs that locate in ribosome stalks: L10Aa/b (dark pink) and LP0/LP0-like (light pink). Paralogs are shown viewed from the front of ribosome.

		Testis 80S			Ovary 80S			
		Paralog in Testis	# aac included in refinement	Resolution (Å)	Paralog in ovary	# aac included in refinement	% identity	RMSD across all atom pairs (Å)
Large subunit	L7/L7-like	L7	226	3.5	L7	226	100	0.481
	L37a/b	L37a	87	3	L37a	87	100	0.514
	L34a/b	L34b	103	3.5	L34b	103	100	0.530
	L24/L24-like	L24	58	3.5	L24	60	100	0.525
	L22/L22-like	**L22-like**	**96**	**4.5**	**L22**	**99**	**57**	**3.107**
Small subunit	S14a/b	S14b	127	5	S14b	127	100	0.797
	S5a/b	**S5a**	**189**	**5.5**	**S5b**	**189**	**90**	**1.805**
	S28a/b	S28b	62	5.5	S28b	62	100	1.990
	S19a/b	**S19b**	**132**	**6**	**S19a**	**126**	**69**	**2.512**

Table 1: Atomic model paralog comparison. Switched paralogs are highlighted in bold.

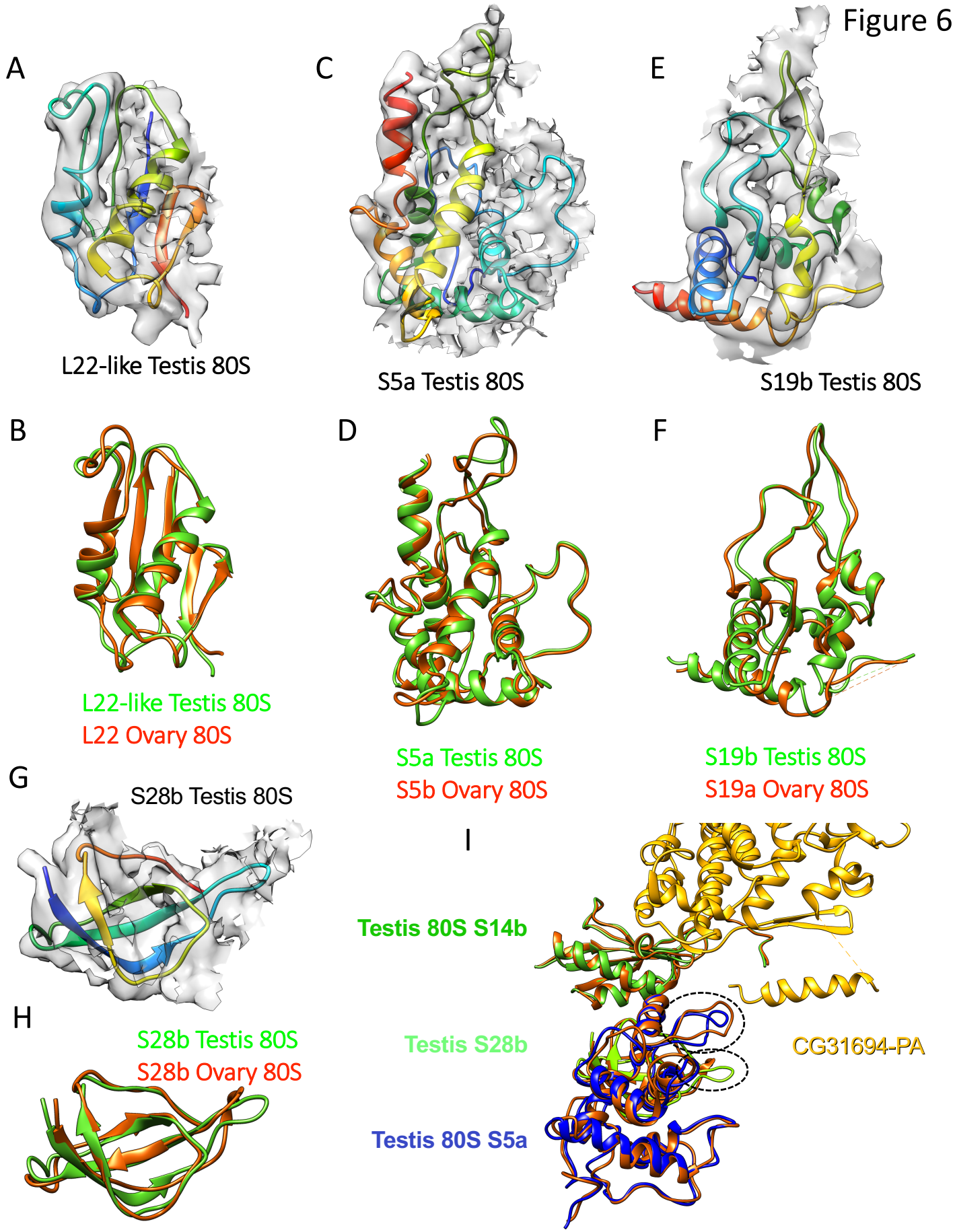

Figure 6: Structural implications of paralog switching events

Switched paralogs in testis 80S vs ovary 80S are shown. (A & B) L22-like (testis 80S) and L22 (ovary 80S). (C & D) S5a (testis 80S) and S5b (ovary 80S). (E & F) S19b (testis 80S) and S19a (ovary 80S). (G & H) S28b (testis 80S) and S28b (ovary 80S). (A, C, E & G) show the testis atomic model fitted into the EM density. The models are rainbow colored from n-terminus (blue) to c-terminus (red). (B, D, F & H) show the comparison between the testis 80S (green) and the ovary 80S (red) atomic models. (I) Area around mRNA channel, which in testis 80S is occupied by an alpha-helix from CG31694-PA. S14b (dark green), S28b (light green) and S5a (blue) from testis 80S are nearby. Ovary 80S paralogs (S14b, S5b and S28b) are superimposed, in red. The main differences between the pdb models, circled, are in regions close to CG31694-PA.

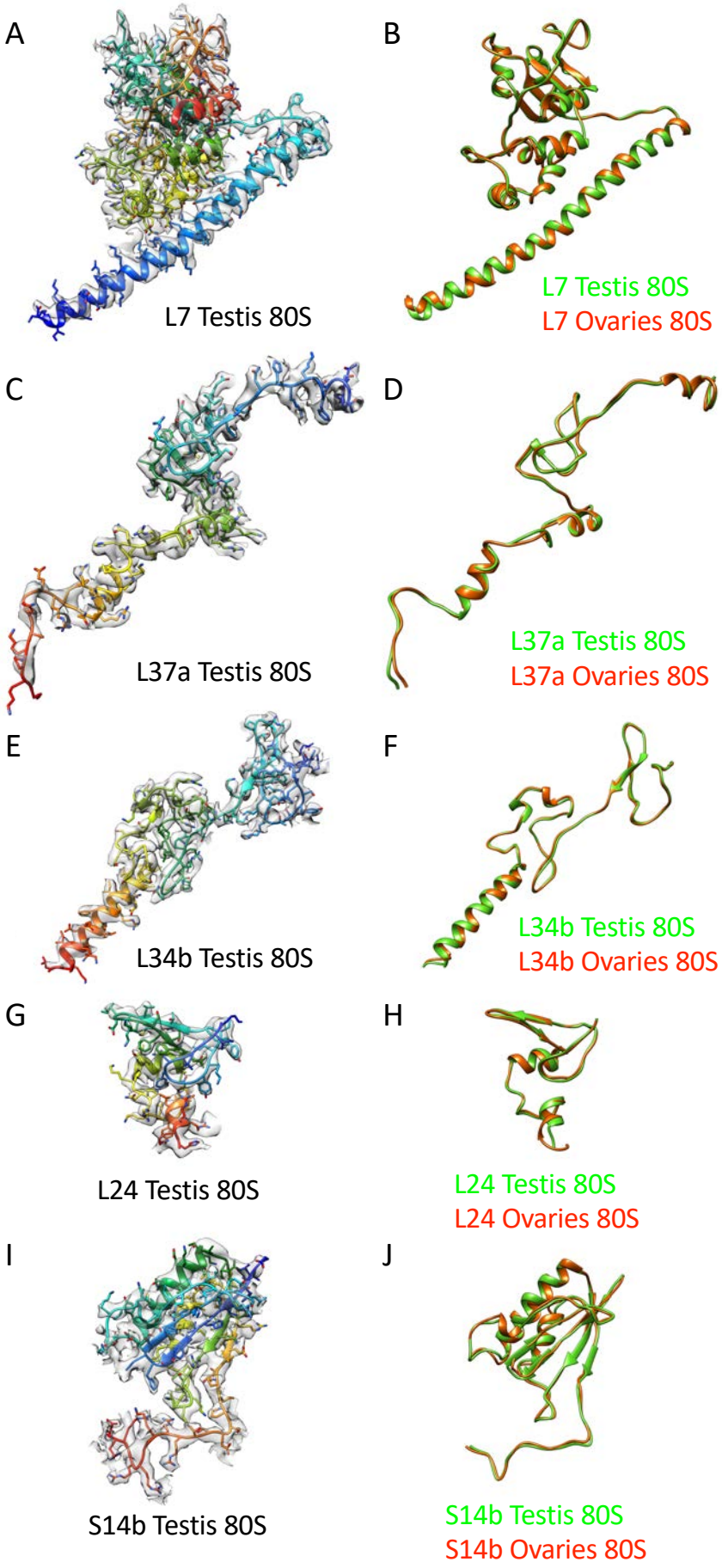

Sup 6: Structural implications of paralog switching events
Non-switched paralogs in Testis 80S vs Ovaries 80S are shown. (A & B) L7; (C & D) L37a; (E & F) L34b; (G & H), L24; (I & J) S14b. (A, C, E, G & I) show the testis atomic model fitted into the EM density. The models are rainbow colored from n-terminus (blue) to c-terminus (red). (B, D, F, H & J) show the comparison between the testis 80S (green) and the ovary 80S (red) atomic models.

Table 2

Paralog 1	Aa length	Paralog 2	Aa length	Amino acid Identity	Specialisation	Human ortholog	Human Disease
RpL22	299	RpL22-like	312	45%	Testis RpL22-like	RpL22 RpL22L1	Cancer/blood disease
RpL37a	93	RpL37b	89	75%	Testis RpL37b	RpL37	
RpS19a	160	RpS19b	159	66%	Testis RpL19b	RpS19	Diamond-Blackfan anaemia. Cancer.
RpS28a	64	RpS28b	65	82%	Testis	RpS28	Diamond-Blackfan anaemia.
RpS10a	163	RpS10b	160	61%	Testis	RpS10	Diamond-Blackfan anaemia. Aase syndrome
RpS5a	228	RpS5b	230	76%	Ovary>Embryo> Testis	RpS5	Diamond-Blackfan anaemia. Cancer.
RpL7	252	RpL7-like	257	28%	Ovary 80S	RpL7	Cancer
RpL24	155	RpL24-like	191	24%	Ovary 80S	RpL24	Tropoblast development

Table 2: Summary of paralog pair attributes
For each paralog pair, amino acid identity, ribosome of specialization, phenotype in *D. melanogaster* mutants, relationship to humans and human diseases.

Figure 7

A

```
CLUSTAL O(1.2.4) multiple sequence alignment

RpL22_dm          MAPTA-KTNKGDTKTAAAKPAEKKAAPAAAAAKGKVEKPKAEAAKP---------AAAAA   50
RpL22-like_dm     MSSQTQKKNASKAK-SKAGPQPSKKAPAKVT---PVETATPSAAPPLSSKKVAKAPAVAL   56
                  *:  : *.* ..:* : * *  .* *** .:    **. . .** *          *.*

RpL22_dm          KNVKKASEAAKDVKAAAAAAAKPAAAKPAAAKPAAASKDAGKKAPAAAAPKKDAKAAAAPA   110
RpL22-like_dm     KNLDLAMKESAK-KAAEAADQKLVS--KAKKGQNASRKNLMQVPEPVAPEVDNKKKSAP-   112
                  **:. * : : . *** ** :  .:   * *   **:.   :.*  .**: * *  :**

RpL22_dm          PAKAAPAKKAASTPAAAPPAKKAAPAKA-------AAPA-AAAPAPAAAAPAVAKPAPKP   162
RpL22-like_dm     -----PKRGNAEIPTVV-PAKKAALVQEKPKEQAAAAPKAENVEVPAAKAKSVKKS---L   163
                       * :  *. *:.. ****** .:        ***    . .*** * :* *

RpL22_dm          KAKAAPAPSKVVKKNVLRGKGQKKKKVSLRFTIDCTNIAEDSIMDVADFEKYIKARLKVN   222
RpL22-like_dm     ATPANPKPKPKRTKNVLRGKRLAKKKAWQRFVIDCACVAEDMILDLADFEQYLKTHIKIK   223
                   : * * *.   .*******   ***.  **.***: :*** *:*:****:*:*:::*::

RpL22_dm          GKVNNLGNNVTFERSK-LKLIVSSDVHFSKAYLKYLTKKYLKKNSLRDWIRVVANEKDSY   281
RpL22-like_dm     NKLNQLKDQVTFERTKNFSLIIHSGVHFSKRYFKYLTKRYLKKVSLRDWLRVVSTAKDTF   283
                  .*:*:* ::*****:* :.**: *.***** *:*****:**** *****:***:. **::

RpL22_dm          ELRYFRISSNDDEDDDAE-----------   299
RpL22-like_dm     AMTYFKIQDKDFDDDDDDVADDNGGKTFA   312
                   : **:*..:* :*** :
```

B

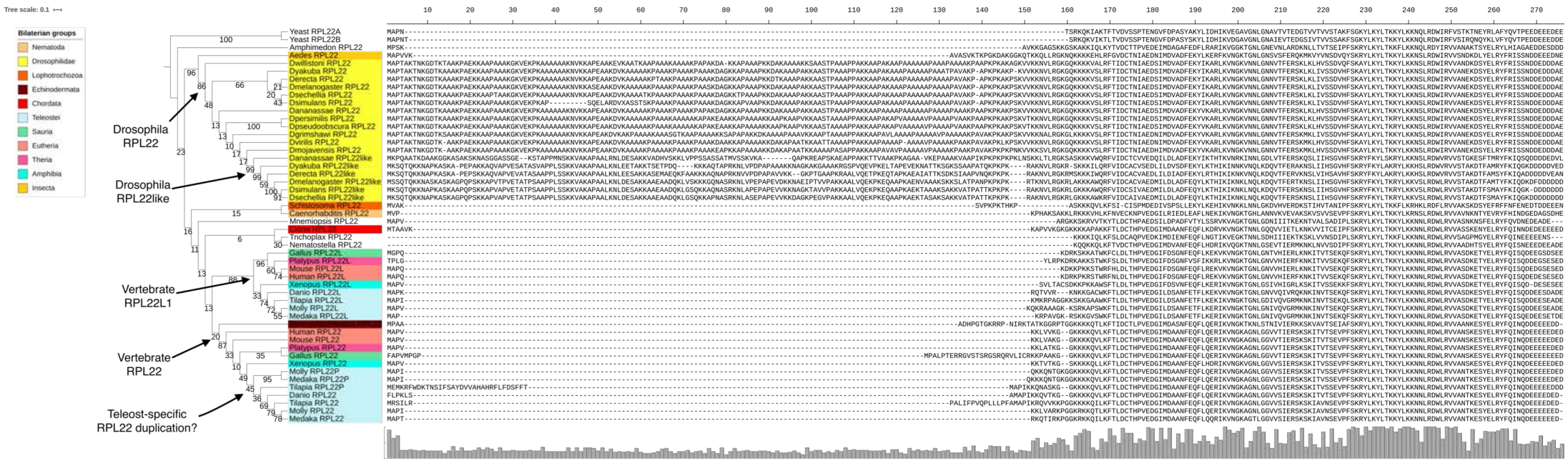

Figure 7: Potential changes to ribosome

A) Alignment of RpL22 and RpL22-like amino acid sequences for the two *D.melanogaster* proteins. In bold, amino acids included in the atomic models. B) Phylogenetic tree for RpL22 and RpL22-like paralogs across a range of animal genomes. The three duplication events detected are indicated.

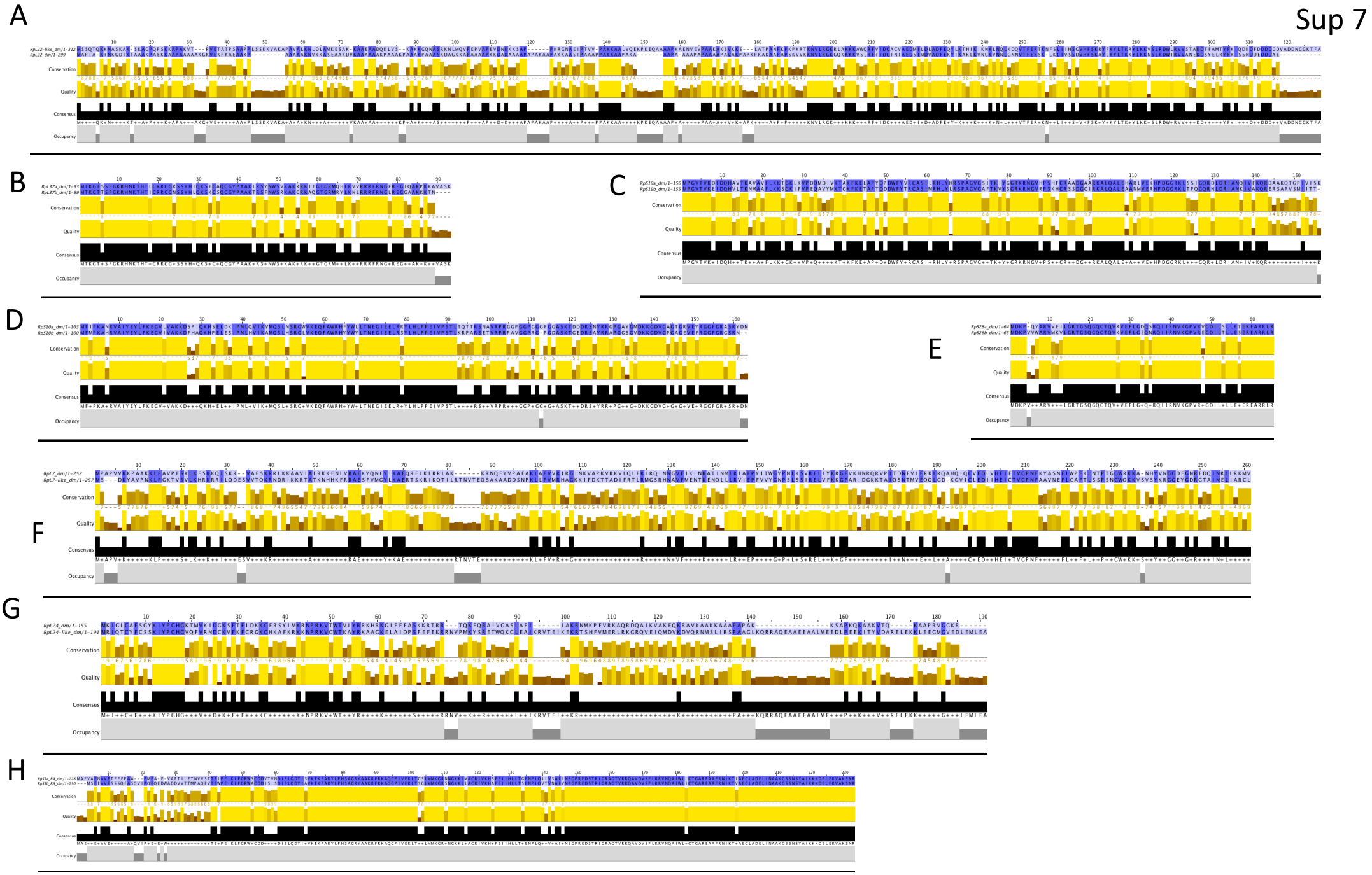

Sup 7: Potential changes to ribosome

Clustal-omega alignment of paralog pairs' protein sequences; A) RpL22/22-like, B) RpL37a/b, C) RpS19a/b, D) RpS10a/b, E) RpS28a/b, F) RpL7/7-like , G) RpL24/24-like, H) RpS5a/b